A fully state- and angle-resolved study of the H+HD→D+H_2 reaction: Comparison of a molecular beam experiment to *ab initio* quantum reaction dynamics

Sheng Der Chao
Institute for Molecular Science, Myodaiji, Okazaki 444-8585 Japan, and Department of Chemistry and Biochemistry, University of Colorado, Boulder, Colorado 80309

Steven A. Harich
Institute of Atomic and Molecular Sciences, Academia Sinica, P.O. Box 23-166, Taipei, Taiwan

Dong Xu Dai and Chia C. Wang
Institute of Atomic and Molecular Sciences, Academia Sinica, P.O. Box 23-166, Taipei, Taiwan and Dalian Institute of Chemical Physics, Chinese Academy of Sciences, Dalian, China

Xueming Yang
Institute of Atomic and Molecular Sciences, Academia Sinica, P.O. Box 23-166, Taipei, Taiwan Dalian Institute of Chemical Physics, Chinese Academy of Sciences, Dalian, China and Department of Chemistry, National Tsing Hua University, Hsinchu, Taiwan

Rex T. Skodje[a)]
Institute for Molecular Science, Myodaiji, Okazaki 444-8585 Japan and Department of Chemistry and Biochemistry, University of Colorado, Boulder, Colorado 80309

(Received 14 March 2002; accepted 11 July 2002)

We present the results of a joint experimental and theoretical investigation of the reaction dynamics of the H+HD→D+H_2 chemical reaction. The experiment was performed using a crossed molecular beam apparatus that employed the Rydberg-atom time-of-flight detection scheme for the product D atom. The photolysis of a HI precursor molecule produced a beam source of hot H atoms, which, when crossed with a cold HD beam, yielded two well-defined center-of-mass collision energies, $E_C = 0.498$ and 1.200 eV. The resolution of the experiment was sufficient to allow the measurement of the rovibrationally state-resolved differential cross section from the ground state of the HD reagent. The reaction was modeled theoretically using a converged coupled channel scattering calculation employing the BKMP2 potential energy surface: The S matrix was computed on a grid of 56 energies in the range $E_C = 0.245 - 1.551$ eV. It is found that the experimental and theoretical state-to-state differential cross sections are in quantitative agreement at the two experimental energies. The geometric phase, which was not included in the calculation, is apparently not required at the energies considered. The spin statistics for the two identical protons is observed to have a dramatic effect on the rotational distribution of H_2 products, giving rise to a saw-toothed distribution with odd-$j' >$ even-j'. The differential cross section for several of the product states exhibited a dramatic forward peak that may be the signature of trapped quantum states near the saddle point. A detailed analysis of the reaction attributes is presented based on the energy dependence of the computed S matrix. © *2002 American Institute of Physics.* [DOI: 10.1063/1.1504083]

I. INTRODUCTION

The H+H_2 reaction and its isotopic variants have been extensively studied over many years.[1–3] Nevertheless, it has only been rather recently that theory and experiment have matured to the point where converged quantum scattering calculations based on an accurate potential energy surface can be brought into agreement with state- and angle-resolved molecular beam measurements.[4–6] A major advance in the design of beam experiments has been the development of the hydrogen Rydberg atom time-of-flight (HRTOF) detection scheme by Welge and co-workers.[4] The HRTOF technique provides an unparalleled level of resolution in the time-of-flight velocity spectrum, which in turn permits very accurate determination of the rovibrationally state-resolved differential cross sections (DCS). We also note there have been other important recent advances in the molecular beam methodology that have allowed improvements in the resolution and facility of reactive scattering data.[5,7–9] On the theory side, a potential energy surface of Boothroyd *et al.*,[10] the BKMP2-PES, is apparently globally accurate to within 30 cm^{-1}, which is likely to be sufficient to model the reaction dynamics. Anderson and co-workers have recently developed an even more accurate surface.[11] Computational reactive scattering algorithms have likewise evolved to a stage where the partial wave expansion of the scattering amplitudes can be converged at energies for which a single potential energy surface is adequate.[12–17] In light of these impressive ad-

[a)]Electronic mail: skodje@spot.colorado.edu

 © 2002 American Institute of Physics

Downloaded 12 Jul 2006 to 203.250.225.116. Redistribution subject to AIP license or copyright, see http://jcp.aip.org/jcp/copyright.jsp

vances, reaction dynamics has passed into a new era where theory and experiment can work much more closely together to study the process of elementary chemical reactions. Detailed comparisons of theory and experiment are far more than an academic exercise, instead providing important synergy impelling both the design of experiment and the focus of theory.

In this work we consider the reaction dynamics of the isotope $H+HD \rightarrow D+H_2$. Curiously, the reaction in this isotope combination has received relatively little attention. On the other hand, the reverse reaction, $D+H_2 \rightarrow H+HD$, and the case $H+D_2 \rightarrow D+HD$, have been studied rather extensively. One reason behind this is the practical issue of experimental signal strength. For the two latter reactions, one expects to observe roughly twice the signal since there are two equivalent reaction paths for homonuclear diatomic reactants. Thus, to this point there has been no report of a molecular beam experiment for the $H+HD \rightarrow D+H_2$ reaction. Similarly, as of yet no converged quantum-mechanical scattering calculation (QM) has been performed. However, a quasiclassical trajectory calculation (QCT) was presented by Hochman-Kowal and Persky[18] on the LSTH and DMBE surfaces. The properties of the transition state have been investigated by Verandas and Yu[19] and, in the reverse reaction $D+H_2 \rightarrow H+HD$, by Truhlar and co-workers.[20] Since the $H+H_2$ system plays such a central role in the field of reaction dynamics, in this work we shall investigate this reaction both experimentally and theoretically. In experiment, the reaction is studied using a crossed molecular beam apparatus that employs the HRTOF detection scheme. A source of hot H atoms is provided by laser photolysis of a HI precursor beam, which yields two collision energies, $E_C = 0.498$ eV and $E_C = 1.200$ eV, corresponding to the two photolysis channels of the precursor. Theoretically, the reaction dynamics is modeled using a coupled channel calculation employing the method of Manolopolous and co-workers[16] and adopting the BKMP2-PES. The calculations were carried out on a fine grid of energies over the range $E_C = 0.245$–1.551 eV which includes the experimental energies. For purposes of analysis, we have also carried out calculations based on reaction path theory, wave packet analysis, spectral quantization, and QCT calculations, which will be presented here and in a companion paper.[21]

While much is known about the $H+H_2$ family of reactions, there remain several outstanding issues that continue to provoke debate. One concerns the role of the geometrical phase[22] (GP) on the reaction dynamics. Kuppermann and co-workers[23] have performed scattering calculations that indicate that the GP can significantly affect the differential cross section in the $D+H_2$ reaction at energies significantly below the conical intersection with the upper surface. Zare and co-workers[5,24] have measured the DCS and integral cross section (ICS) experimentally. Kuppermann and Wu[25] have found that the DCS was in better agreement with calculations including the GP than those without the GP. Thereafter, Welge and co-workers[4] studied the same reaction using the HRTOF detection method in a molecular beam experiment and arrived at the opposite conclusion. Recently, Kendrick[26] has claimed that the influence of the GP should largely cancel out due to equal and opposite contributions from neighboring values of the total angular momentum (J). However, that analysis was restricted to low values of J and may not hold for higher J. In fact, the recent results of Kuppermann and Wu[27] strongly suggest that this cancellation will not occur at high J. Therefore, it is of great interest to determine whether a calculation without the GP (such as our treatment here) is adequate to reproduce experiment in the case of the H+HD reaction. Obviously the GP should be introduced in an exact calculation; however, it is an open question as to the minimum collision energy required for it to have an observable effect.

Another outstanding issue concerns the role of reactive resonances.[28,29] While the existence of reactive resonances has been long predicted based on theoretical simulations,[30,31] it has proven to be quite difficult to observe in collision experiments. It is well understood that impact parameter averaging effectively smears the resonance over a large energy range, making it very challenging to identify in reactive cross sections.[32] In fact, it was only very recently[33,34] that a clear resonance signature was observed in any bimolecular reaction, i.e., $F+HD \rightarrow D+HF$, and for that case it was clearly observed only because it was narrow, isolated, and occurred below the threshold for direct reaction. The $H+H_2$ resonances are much more difficult to observe since they lie at fairly high energies and, according to theoretical estimates,[35–37] are extremely short lived, <20 fs. (However, when the GP is included, there is evidence that certain resonance states may have much longer lifetimes.[25,38]) Miller and Zhang[39] have suggested using a resonance ridge of the differential cross section (DCS) in the energy-angle plane as the fingerprint of a reactive resonance. However, the J shifting of other features, such as adiabatic barriers, can lead to similar ridges not easily distinguished from resonance ridges; furthermore, the ridge structures are seen to occur in quasiclassical trajectory studies as well.[40] Other ideas involve the search for anomalous forward peaks in the DCS, or unusual characteristics of product branching ratios. While a general resonance signature is as of yet unknown, it is clear that state- and/or angle-resolved measurements are required. Recently, Shafer-Ray and co-workers[41] observed a peak in the integral cross section (ICS) versus energy for the reaction $H+D_2 \rightarrow D+HD$ $(v'=0, j'=7)$, which also appeared in the calculations of Kendrick, that seemed to indicate resonance. To investigate the proposed resonance interpretation, we[42] (and also Aoiz *et al.*[43] and Kendrick[44]) have performed a fully converged quantum scattering calculation wherein the theoretical peak disappeared, suggesting the observation might be an artifact of the experimental sensitivity function. In a different experiment, however, Zare and co-workers[45] have observed a forward peak in the DCS for the $H+D_2$ $(v=j=0) \rightarrow HD(v'=3, j'=0)+H$ reaction at total energy 1.83 eV. A quasiclassical trajectory calculation accompanying the experiment and a subsequent analysis using the adiabatic theory[46] tend to support the resonance interpretation. More recently, we have also observed such forward peaks both experimentally and theoretically for the title reaction.[47,48] Still at issue is whether an unambiguous interpretation based on resonances can be solely responsible for

Downloaded 12 Jul 2006 to 203.250.225.116. Redistribution subject to AIP license or copyright, see http://jcp.aip.org/jcp/copyright.jsp

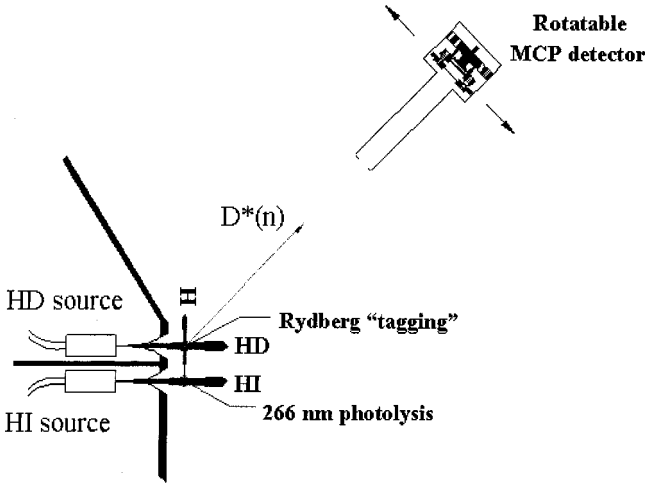

FIG. 1. A schematic diagram of the experimental apparatus.

the observed angular distribution. In any case, close interaction between experiments and theory has been critical in the ongoing debate.

Finally, we note the interesting role of spin statistics in the H+HD→H_2+D reaction. To achieve the correct Fermi–Dirac (FD) nuclear statistics for the final $H_2(v',j')$ product molecule, *para* spin states occur only with j' = even rotational states, while *ortho* spin states occur only with j' = odd states. As noted earlier by Zare and co-workers[49] for the reaction H+HI→I+H_2, this can lead to dramatic effects on the final rotationally resolved product distribution. With the high level of energy resolution of the HRTOF technique employed here, it is possible to test whether the dramatic saw-toothed rotational distribution seen by Rinnen *et al.*[49] occurs in the present case.

The paper is organized as follows: In Sec. II, we describe the experimental apparatus and the procedures used to obtain cross sections from the observed signals. In Sec. III, the theoretical methodology of the scattering calculations is discussed. The results of the scattering calculations and the experiment for the two beam energies are presented in Sec. IV. In Sec. V, the theoretical scattering dynamics over the full energy range is analyzed. Finally, Sec. VI presents a brief summary of our conclusions. For purposes of brevity, most of the discussion of reactive resonance will be deferred to a later paper.

II. EXPERIMENTAL METHOD

In this work, the H+HD→H_2+D reaction was studied experimentally with a molecular beam apparatus using the H(D) Rydberg-atom ''tagging'' time-of-flight (HRTOF) technique, which was originally developed by Welge and co-workers.[50] The experimental apparatus employed in this study is the same one used previously in a study of the $O(^1D)+H_2$ reaction.[51,52] Figure 1 shows the experimental scheme used in this work. The excitation of the ground-state $D(1s)$-atom product to its Rydberg state is made by a two-step excitation scheme. The 121.6 nm vacuum ultraviolet (VUV) light used in the first step excitation of the $D(1s)$ atom to the $2p$ level is generated by a two photon resonant $(2\omega_1-\omega_2)$ four wave mixing scheme in the Kr-gas cell. In this scheme, $2\omega_1$ (212.5 nm) is resonant with the Kr $(4p-5p)$ transition.[53] The ω_1 light is generated by doubling the output of a dye laser pumped by a Nd:YAG (355 nm) laser, while the ω_2 (845 nm) light is the direct output of a dye laser pumped by the second harmonic of the same YAG laser. Several mJ of 212.5 and 845 nm laser light are typically used in the experiment. By generating about 50 μJ of the 121.6 nm laser light, the first step can be easily saturated since this transition has a very large excitation cross section $(3.0\times10^{-13}$ cm$^2)$. Following the excitation, the $D(2p)$ atom product is then sequentially excited to a higher Rydberg state with $n\approx50$ using 365 nm light, which is generated by doubling a dye laser pumped by the same YAG laser. These two excitation laser pulses are overlapped well in space and synchronized in time in the detection region. The neutral Rydberg D atom then travels a certain TOF distance before reaching an MCP detector with a fine metal grid (grounded) in the front. After passing through the grid, the Rydberg D atoms are immediately field ionized by the electric field applied between the front plate of the Z-stack multichannel plate (MCP) detector and the fine metal grid, and detected by the Z-MCP detector.

Two parallel molecular beams (HI and HD) are generated with similar pulsed valves in this experiment. The H-atom beam is produced by photolysis of the HI molecule at 266 nm using a Nd:YAG fourth-harmonic laser output. There are two different photolysis channels, corresponding to the two spin–orbit states of the iodine atom, which give rise to two sharp peaks of H-atom velocity distribution: a fast component at 17 470 m/s and a slow component at 11 230 m/s. The H beam is then crossed at 90° with the HD molecular beam. The HD beam was produced by an adiabatic expansion through a nozzle cooled to liquid nitrogen temperatures. Almost of all the HD molecules in the beam are in the ground rovibrational state, $(v,j)=(0,0)$. Using the fast and slow HI photolysis channels separately, two collision energies could be obtained: $E_C=0.498$ and 1.200 eV, which correspond to the total system energies: $E=0.733$ and 1.435 eV, if the HD zero-point energy is included. The spread in translational energies was estimated to be $\Delta E_C=10$ and 15 meV, respectively. The D-atom products were detected using a rotatable MCP detector that permits the determination of the DCS over the full angular range.

TOF spectra of D atom at different laboratory scattering angles were measured using the techniques described. For the collision energy of 0.498 eV, Fig. 2 shows six typical TOF spectra at different laboratory angles. These TOF spectra can be converted to the product translational energy distributions employing an algorithm for the LAB-to-c.o.m. conversion. In Fig. 3, we show four typical distributions that were obtained. Similar TOF spectra and translational energy distributions for the high collision energy, 1.200 eV, are shown in Figs. 4 and 5. A great deal of effort was expended to measure scattering at the LAB angles corresponding to forward scattering in the c.o.m.; this proved difficult because of the unfavorable kinematics and also signal attenuation due to the HI beam. Indeed, the forward scattering of the high internal energy products was very close in the LAB frame to

Downloaded 12 Jul 2006 to 203.250.225.116. Redistribution subject to AIP license or copyright, see http://jcp.aip.org/jcp/copyright.jsp

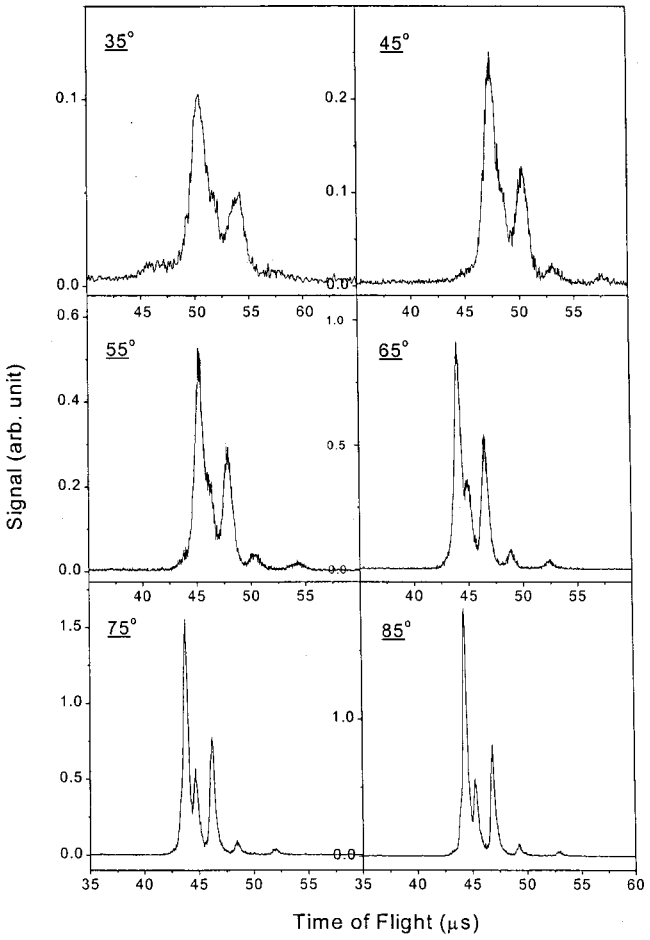

FIG. 2. Time-of-flight spectra recorded at $E_C=0.498$ eV for $H+HD\rightarrow D+H_2$ for six LAB angles, defined using the HD beam as 0°. The peak structures observed in the spectra correspond to rotational states of the H_2 product molecule.

the unscattered beam direction. Figure 6 shows the TOF spectrum of the D atom at $E_C=1.200$ eV for the laboratory angle of $-58°$, which is the forward scattering direction for the $v'=0$ H_2 product, along with the translational energy distribution converted from this TOF spectrum. Despite the experimental difficulties, it is clear that an assignable TOF can be obtained for forward scattering of the $H_2(v'=0)$ product states. The forward scattering is dominated by the $j'=0-2$ rotational states. For the $H_2(v'=1)$ product states at $E_C=1.200$ eV, the presence of a very large background prevented the accurate determination of forward scattering TOF spectrum. For the low energy collision, $E_C=0.498$ eV, no forward scattering was observed.

The sharp structures in the TOF spectra and the translational energy distributions can be assigned to different H_2 (v',j')-product states from the H+HD reaction, which, in turn, determine the relative state-resolved differential cross sections. An experimental apparatus function based on a realistic experimental model is used to calibrate the signals at different detection time delays and laboratory angles. These calibrations are essentially determined in the same manner as previously done by Welge and co-workers.[4] The results of the data analysis are the relative state-to-state differential cross sections. To obtain actual numerical values, a single scaling factor taken from the theoretical scattering calculations is multiplied times the experimental results. This factor, which was used for both energies and for all angles and states, was chosen to optimize the agreement between the experimental and theoretical ICS. The state-to-state ICS are obtained by numerically integrating the DCS over solid angle. The experimental results for the DCS and ICS will be presented and discussed in Sec. IV.

III. QUANTUM REACTION DYNAMICS

The present quantum-mechanical calculations (QM) were performed using the same quantum reactive scattering methods as in previous works[16,33,42,54] and employed the BKMP2-PES. The method used a time-independent coupled channel hyperspherical coordinate method similar to that of Schatz,[55] with a technique to avoid overcompleteness problems in the exchange region as described by Parker and Pack.[56] The coupled channel equations are solved with a

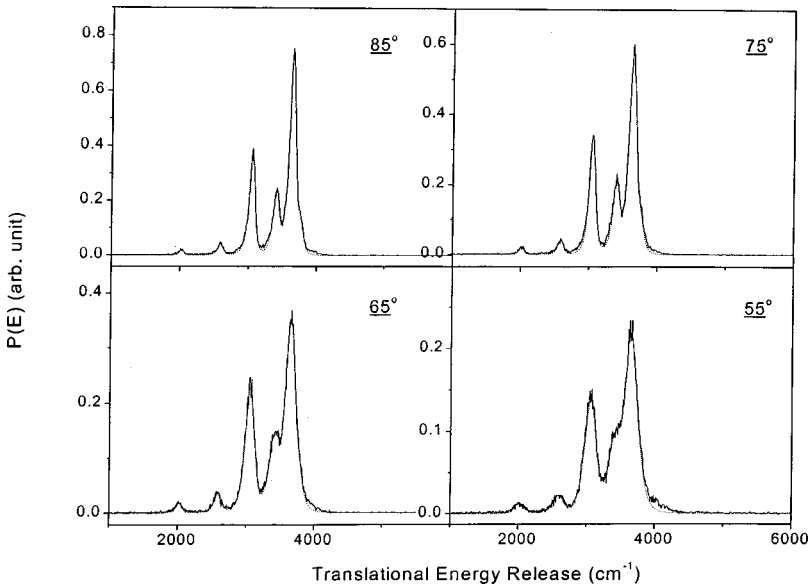

FIG. 3. The translational energy distributions for four of the TOF spectra shown in Fig. 2 for the case $E_C=0.498$ eV.

Downloaded 12 Jul 2006 to 203.250.225.116. Redistribution subject to AIP license or copyright, see http://jcp.aip.org/jcp/copyright.jsp

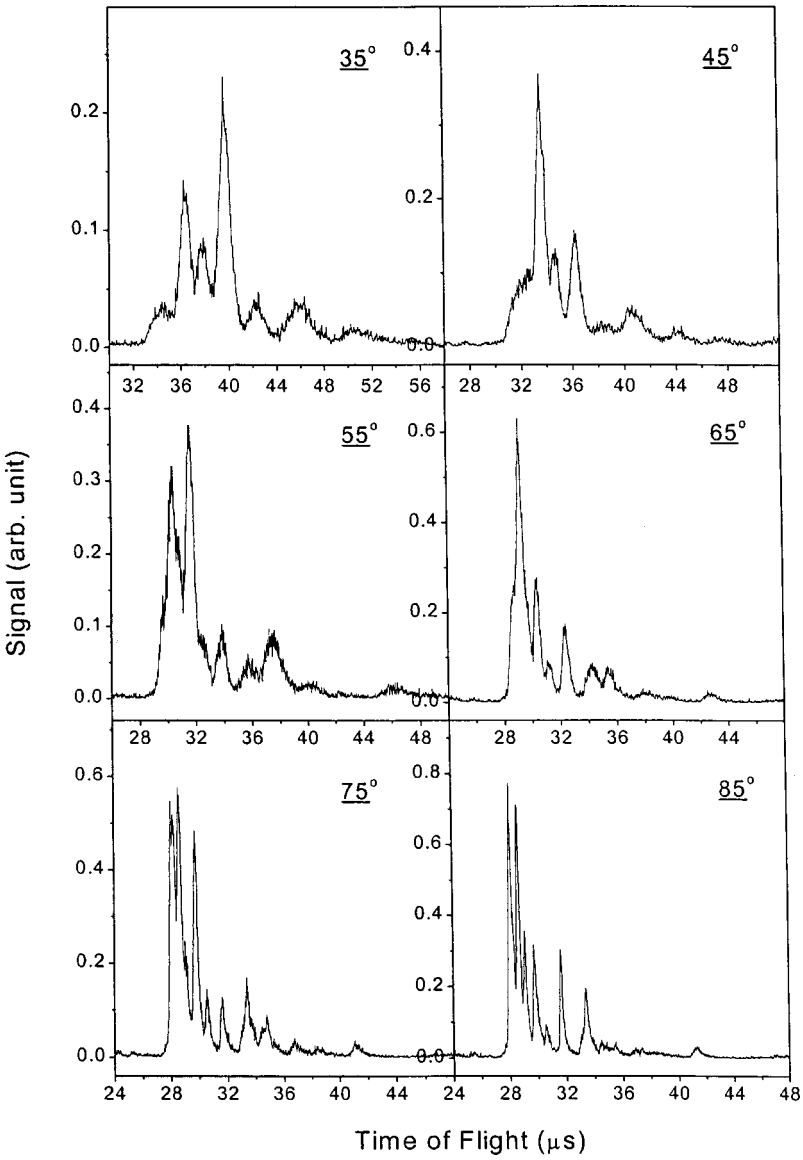

FIG. 4. Time-of-flight spectra recorded at $E_C=1.200$ eV for H+HD→D+H_2 for six LAB angles. The peak structures observed in the spectra correspond to rovibrational states of the H_2 product molecule.

modified log-derivative propagator.[57] The calculations introduce no approximation into the rotational dynamics beyond the finite basis set. For nonzero total angular momenta ($J>0$), the method uses a parity-adapted body-fixed axes formulation as described elsewhere,[58] which retains all the basis functions with helicity quantum numbers $k \leqslant \min(J, j, k_{\max})$ in each arrangement.

Although the experiments were carried out at just two collision energies, it is important to obtain the variation of reaction attributes as a function of energy to obtain a physical understanding of the reaction dynamics. Thus, the S matrix for the H+HD reaction was computed at 56 grid energies with resolutions 0.024 eV for $E=0.48-1.79$ eV, including zero-point energy. In the present calculation, we focus on the lowest reactant state, HD($v=j=0$) only, which is sufficient to model the experimental results. However, the full S matrix was computed for the case $J=0$ for purposes of analysis. For the HD(0,0) state, the calculations were performed for total angular momentum quantum number, J, up to $J_{\max}=35$ in order to give well-converged angular distributions at high energies. The three key convergence parameters in this calculation are denoted $E_{\max}$, $j_{\max}$, and $k_{\max}$. The first two parameters define the coupled channel basis set, where all the channels with diatomic energy levels less than or equal to $E_{\max}$ and rotational quantum numbers less than or equal to $j_{\max}$ are included. The third parameter $k_{\max}$ sets an upper limit on the helicity quantum number k and is only relevant for higher J. Tables I(a) and I(b) show the convergence of selected $J=0$ reactive reaction probabilities for the H+D_2($v=0$, $j=0$) reaction as a function of $E_{\max}$ and $j_{\max}$, respectively. It was found that the reaction probabilities are well-converged with $E_{\max}=2.5$ eV and $j_{\max}=16$, which are the values of these parameters we used in our calculations. Convergence tests on the parameters $k_{\max}$ have been performed for several selected J and total energy E, and some of the results are shown in Table I(c). It can be seen that the dominate reaction probabilities are all well-converged by using $k_{\max}=6$, while using a value $k_{\max}=7$ gives the same reaction probabilities with differences smaller than 2%, even for higher energies. Another parameter, $mtr=200$, denoting the number of sectors in log-derivative propagation, was also

Downloaded 12 Jul 2006 to 203.250.225.116. Redistribution subject to AIP license or copyright, see http://jcp.aip.org/jcp/copyright.jsp

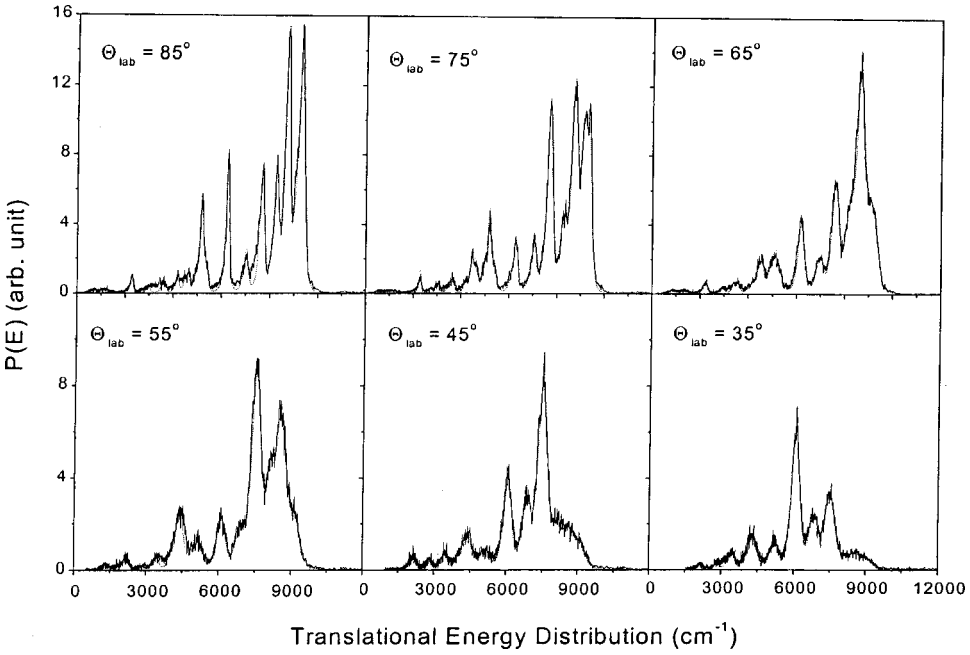

FIG. 5. The translational energy distributions for the TOF spectra shown in Fig. 4 for the case $E_C = 1.200$ eV.

tested. It was found the results were fairly sensitive to mtr and required care in choosing a sufficiently large value. We have also tested the convergence of the DCS. For final product states that are significantly populated in the reaction, it was found that the DCS was converged to within 5% except at the highest energies.

Having calculated the S-matrix elements, we can generate the state-to-state ICS and DCS by using the standard helicity representation formulas;[12] see below. The DCS is computed using the scattering angle $\pi-\theta$ instead of θ, which agrees with the modern experimental definition with the forward scattering referring to the final velocity vector of product diatomic molecule lying parallel to the initial velocity vector of the H atom in the center-of-mass frame.

To compare with experiment, it is important to consider the role of spin statistics in the scattering process. In the reaction $H+HD(v,j)\rightarrow D+H_2(v',j')$, Fermi–Dirac (FD) statistics requires that $j'=$odd for *ortho* spin states of $H_2(v',j')$ product, while $j'=$even for the *para* spin states. However, the numerical scattering calculations are carried out without regard to particle spin (i.e., Boltzmann statistics), and so the resulting S matrix is a superposition of *para* and *ortho* components. Nevertheless, it is a relatively straightforward matter to disentangle the separate contributions and produce the quantity that should be compared to the experimental molecular beam results. Using the postantisymmetrization procedure discussed by Kuppermann and co-workers[59] (also see Zhang and Miller[12]), we construct the correct FD amplitudes using combinations of the computed (Boltzmann) amplitudes. It is assumed that a statistical mixture of $\frac{1}{4}$ *para* and $\frac{3}{4}$ *ortho* states exists in the initial beam, and that the proton spins are essentially uncoupled to the reaction dynamics, which thus persists into the final (or post) scattering region. For distinguishable atoms, we label the arrangement channels $H+H'D$, $H'+HD$, and $D+HH'$ as α, β, and γ, respectively, and the computed Boltzmann scattering amplitudes are denoted by $S_B^{\alpha\rightarrow\beta}(v,j\rightarrow v',j')$, etc. For a given spin state, χ, the correct FD spatial scattering wave function, $|\Psi_{\rm FD}+\rangle$, has odd symmetry with respect to proton interchange for χ_{ortho} and even symmetry for χ_{para}. Thus, $|\Psi_{\rm FD}+\rangle$ is a superposition of the $\alpha\rightarrow\gamma$ and $\beta\rightarrow\gamma$ wave functions produced by the numerical algorithm, i.e.,

$$|\Psi_{\rm FD}+\rangle=\frac{1}{\sqrt{2}}(|\Psi_B^{\alpha\rightarrow\gamma}+\rangle\pm|\Psi_B^{\beta\rightarrow\gamma}+\rangle), \tag{3.1}$$

where $-$ is used for *ortho* states and $+$ with *para* states. Obviously, $|\Psi_B^{\alpha\rightarrow\gamma}+\rangle$ and $|\Psi_B^{\beta\rightarrow\gamma}+\rangle$ are physically identical except that the H_2 internuclear vector, $\boldsymbol{r}$, is replaced by $-\boldsymbol{r}$. Asymptotically in the γ channel, the scattering amplitudes are thus equal for $j'=$even, and equal in magnitude but opposite sign for $j'=$odd. This implies for a single *para* (*ortho*) spin state

$$S_{\rm FD}(H+DH\rightarrow D+H_2) = \sqrt{2}\times\begin{vmatrix} S_B^{\alpha\rightarrow\gamma}(v,j\rightarrow v',j') & j'=\text{even (odd)} \\ 0 & j'=\text{odd (even)}. \end{vmatrix} \tag{3.2}$$

Including the statistical weights for the spin states, the cross sections (either ICS or DCS) are thus given by

$$\sigma_{\rm FD}(H+DH\rightarrow D+H_2)=\begin{vmatrix} \frac{1}{2}\sigma_B^{\alpha\rightarrow\gamma}(v,j\rightarrow v',j') & j'=\text{even} \\ \frac{3}{2}\sigma_B^{\alpha\rightarrow\gamma}(v,j\rightarrow v',j') & j'=\text{odd}. \end{vmatrix} \tag{3.3}$$

Hence, we expect a difference of roughly a factor of 3 between the production rates for neighboring odd and even rotational states of H_2.

The state-to-state differential cross sections are obtained using the expression

Downloaded 12 Jul 2006 to 203.250.225.116. Redistribution subject to AIP license or copyright, see http://jcp.aip.org/jcp/copyright.jsp

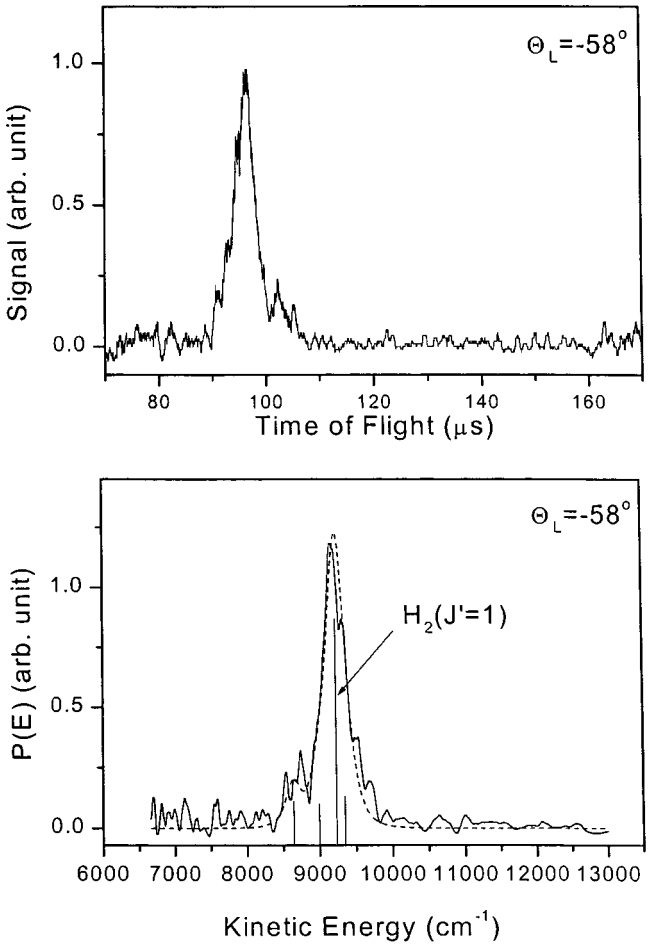

FIG. 6. The time-of-flight spectrum and the translational energy distribution for the LAB angle of −58° for $E_C=1.200$ eV. This LAB angle corresponds to forward scattering in the c.o.m. frame.

$$\frac{d\sigma_R(v,j,k\rightarrow v',j',k')}{d\Omega} = \frac{p_{j'}}{4k_{vj}^2}\left|\sum_J (2J+1)\cdot d^J_{k,k'}(\pi-\theta) \cdot S_B^{\alpha\rightarrow\gamma}(v,j,k\rightarrow v',j',k')\right|^2, \tag{3.4}$$

where (v,j,k) are the quantum numbers for the reactant or (primed) product states, $p_{j'}$ are the FD weighting factors, and S is computed using Boltzmann statistics. When the helicity is unobserved, as in the present experiments, the DCS is obtained using the usual averaging procedure

$$\frac{d\sigma_R(v,j\rightarrow v',j')}{d\Omega} = \frac{1}{2j+1}\cdot\sum_{k,k'}\frac{d\sigma_R(v,j,k\rightarrow v',j',k')}{d\Omega}. \tag{3.5}$$

Finally, to provide a measure of physical insight into the reaction dynamics, we have also implemented a simple vibrationally adiabatic model based on natural collision coordinates. Following procedures outlined by Miller *et al.*[60] and Isaacson *et al.*,[61] we constructed the minimum energy path (MEP) which passes through the H–H–D saddle point on the BKMP2-PES. The vibrationally adiabatic potential curves, $V_{\rm adi}(s;\boldsymbol{n})$, are constructed in a simple way, based on a normal mode analysis of the projected force constant matrix

$$V_{\rm adi}(s;\mathbf{n}) = V_{\rm MEP}(s) + \varepsilon_{\rm vib}(s;\mathbf{n}). \tag{3.6}$$

TABLE I. (a) Convergence test of selected H+HD($v=0$, $j=0$)→H_2+D reaction probabilities as a function of $E_{\rm max}$ (with $J=0$, $E_{\rm tot}=1.7$ eV, and $j_{\rm max}=16$). (b) Convergence test of selected H+HD($v=0$, $j=0$)→H_2+D reaction probabilities as a function of $j_{\rm max}$ (with $J=0$, $E_{\rm tot}=1.7$ eV, and $E_{\rm max}=2.5$ eV). (c) Convergence test of selected H+HD($v=0$, $j=0$)→H_2+D reaction probabilities as a function of $k_{\rm max}$ (with $E_{\rm max}=2.5$ eV and $j_{\rm max}=16$).

		$H_2(v',\text{all } j')+D$			
(a) $E_{\rm max}$		$v'=0$	$v'=1$	$v'=2$	$v'=3$
2.4		0.176 92	0.037 35	0.006 17	0.000 00
2.5		0.176 70	0.037 26	0.006 20	0.000 00
2.6		0.176 64	0.037 28	0.006 24	0.000 00
		$H_2(v',\text{all } j')+D$			
(b) $j_{\rm max}$		$v'=0$	$v'=1$	$v'=2$	$v'=3$
15		0.176 88	0.037 36	0.006 23	0.000 00
16		0.176 70	0.037 26	0.006 20	0.000 00
17		0.176 64	0.037 24	0.006 19	0.000 00
	$E_{\rm tot}=1.7$ eV	$H_2(v',\text{all } j')+D$			
(c) J	$k_{\rm max}$	$v'=0$	$v'=1$	$v'=2$	$v'=3$
20	5	0.079 15	0.025 11	0.002 33	0.000 00
	6	0.082 31	0.023 96	0.002 41	0.000 00
	7	0.083 53	0.023 62	0.002 43	0.000 00

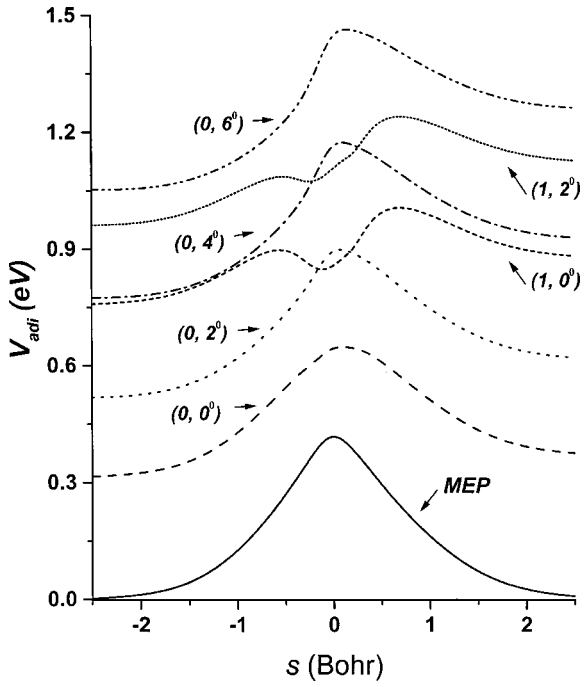

FIG. 7. The vibrationally adiabatic potential curves for the $J=0$ dynamics of the H+HD→D+H_2 reaction on the BKMP2-PES. The coordinate s measures length along the MEP in mass-weighted coordinates and is set to $s=0$ at the saddle point. The lowest curve is $V_{\rm MEP}(s)$.

Downloaded 12 Jul 2006 to 203.250.225.116. Redistribution subject to AIP license or copyright, see http://jcp.aip.org/jcp/copyright.jsp

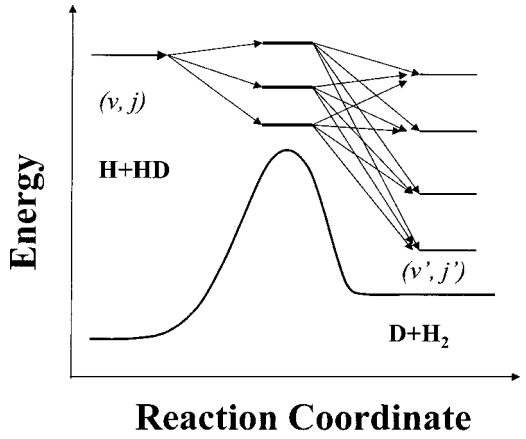

FIG. 8. A schematic diagram of state-to-state reaction dynamics in the vibrationally adiabatic basis. Due to nonadiabatic coupling, the incident flux of reactants is distributed over a number of adiabatic curves, leading to the view that several adiabatic barriers may leave an imprint on individual state-to-state reaction probabilities.

In Eq. (3.6), the coordinate s is the distance along the MEP in mass scaled coordinates and $V_{\mathrm{MEP}}(s)$ is the BKMP2-PES evaluated on the MEP. The vibrational energies, in the separable-mode approximation $\varepsilon_{\mathrm{vib}}(s;\boldsymbol{n})$, are computed using a local Morse approximation for the symmetric stretch and the exact quantum levels for the bend. For our purposes, Eq. (3.6) is sufficient to provide the approximate positions of adiabatic barriers (quantized bottlenecks) and wells to aid in the physical analysis of the energy dependence of the QM scattering results. We should note that coupling between the modes is quantitatively significant and that the true bottleneck energies are shifted (downward) particularly for highly bend-excited species.

In Fig. 7, we plot the adiabatic curves for H+HD $\rightarrow$D+H_2 that are consistent with total angular momentum $J=0$. The bend levels are restricted to the even quantum numbers for $J=0$, but the odd bend levels will play a role for $J>0$. [Of course, one also expects that for $J>0$ the adiabatic curves will be "J-shifted" by an amount $\sim\hbar^2 J(J+1)/2I(s)$.] The lowest bottleneck to reaction is provided by the barrier on the ground adiabatic curve, $(v_{ss}, V^{\Lambda}_{\mathrm{bend}})=(0,0^0)$, which lies at a total energy of $E=0.65$ eV. Here, Λ is the vibrational angular momentum. The bend excited curves for $(0,2^0)$, $(0,4^0)$, and $(0,6^0)$ are simple barriers with peaks near the saddle point value $s=0$, and exhibit spacings of $2\hbar\omega_{\mathrm{bend}}=0.22$ eV. The symmetric stretch excited curve,

TABLE II. Comparison of the theoretical and experimental integral cross sections in Å^2 for H+HD $(v=j=0)\rightarrow$D+H_2 $(v'=0,1;j')$ for collision energies $E_C=0.5$ and 1.2 eV.

	$v'=0$, $E_c=0.5$ eV		$v'=0$, $E_c=1.2$ eV		$v'=1$, $E_c=1.2$ eV	
j'	QM	Expt.	QM	Expt.	QM	Expt.
0	0.011 38	0.011 56	0.003 17	0.003 24	0.001 20	0.000 08
1	0.079 77	0.081 48	0.028 19	0.022 09	0.011 33	0.008 11
2	0.026 11	0.025 02	0.015 32	0.015 72	0.006 20	0.005 85
3	0.046 89	0.046 40	0.063 34	0.058 41	0.022 44	0.021 14
4	0.005 71	0.006 82	0.027 91	0.026 30	0.006 86	0.009 74
5	0.003 20	0.004 08	0.108 65	0.103 23	0.014 86	0.016 89
6			0.041 51	0.041 84	0.003 51	0.004 89
7			0.111 92	0.114 33	0.007 09	0.009 84
8			0.024 61	0.025 14		
9			0.034 76	0.034 60		

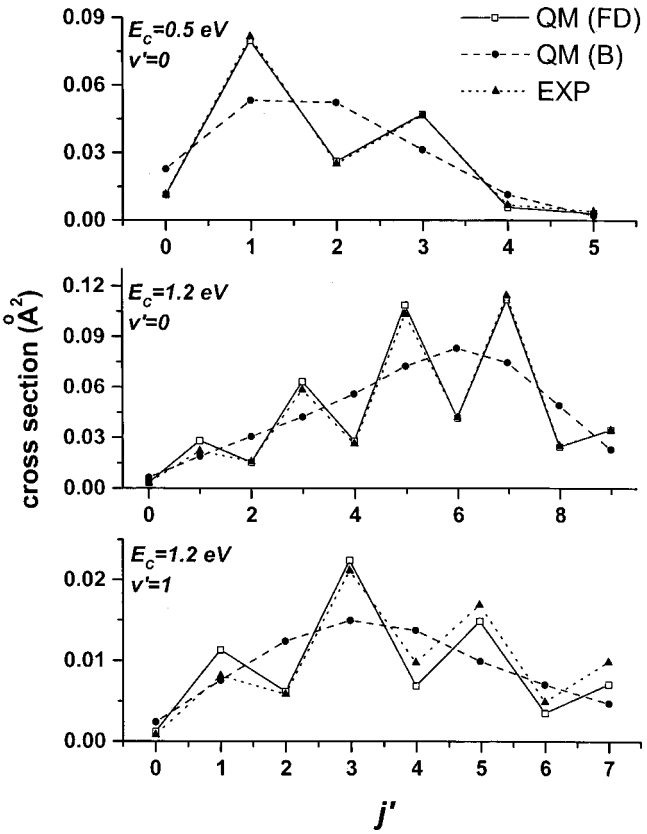

FIG. 9. The ICS in Å^2 for H+HD$(v=0,\ j=0)\rightarrow$D+$H_2(v',j')$ vs j' at the two collision energies. The dotted lines are the experimental results and the solid lines represent the results of QM with FD statistics. The dashed lines are the (artificial) distributions obtained using Boltzmann statistics.

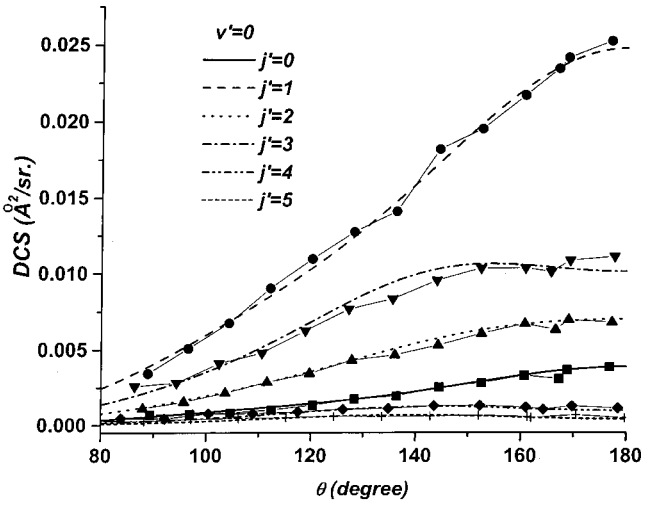

FIG. 10. The DCS in Å$^2/sr$ for H+HD$(v=0,\ j=0)\rightarrow$D+$H_2(v',j')$ vs c.o.m. scattering angle Å^2. The symbols are the experimental results, normalized as in Fig. 9, while the solid lines are the results of QM. The upper panel is the low collision energy, $E_C=0.498$ eV, for $v'=0$. The lower panels are for $E_C=1.200$ eV with $v'=0,1$, respectively. Typical experimental error bars are $<10\%$.

Downloaded 12 Jul 2006 to 203.250.225.116. Redistribution subject to AIP license or copyright, see http://jcp.aip.org/jcp/copyright.jsp

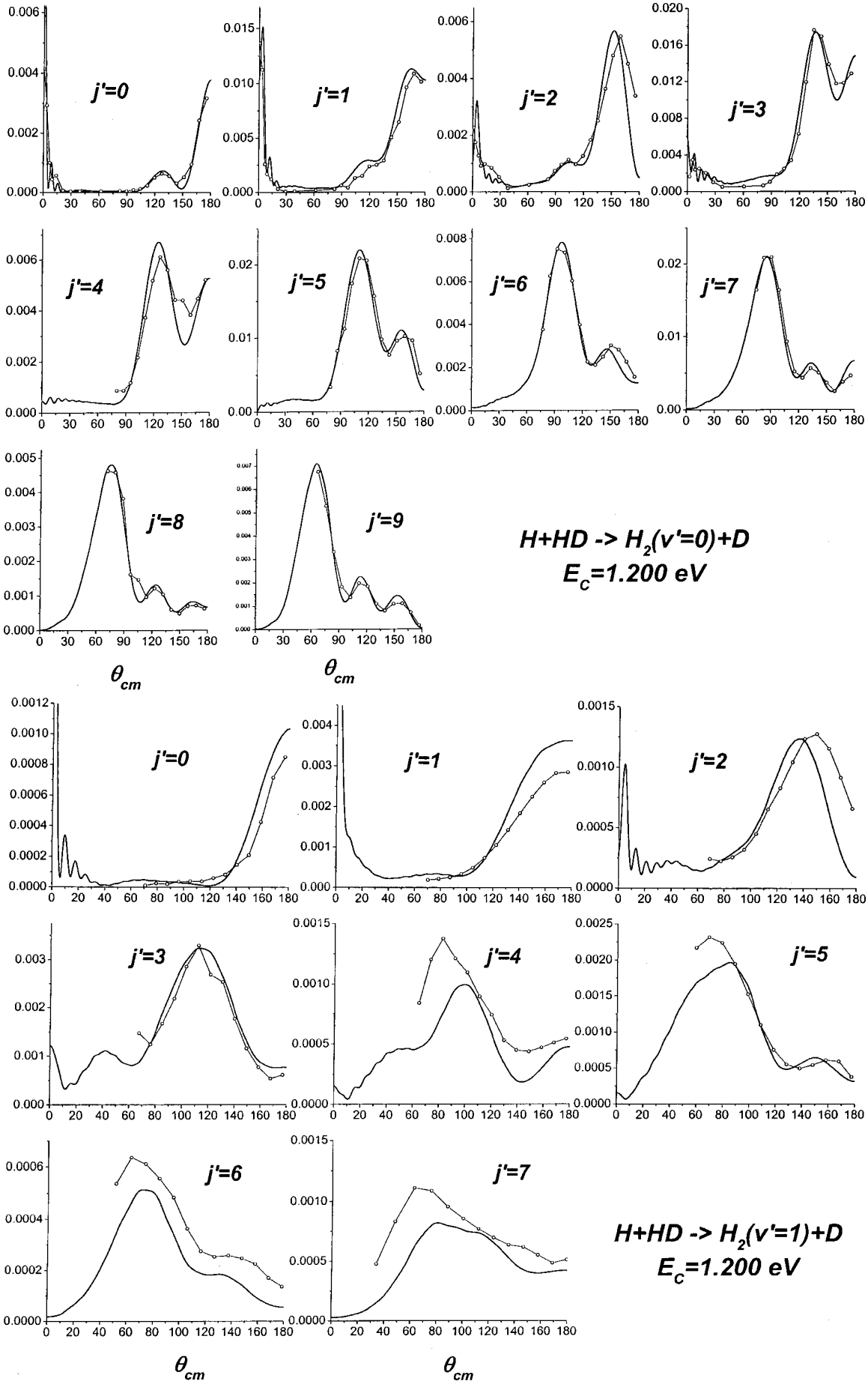

FIG. 10. (*Continued.*)

Downloaded 12 Jul 2006 to 203.250.225.116. Redistribution subject to AIP license or copyright, see http://jcp.aip.org/jcp/copyright.jsp

for the state $(1,0^0)$, shows an asymmetrical double barrier enclosing a shallow well. The higher barrier is on the product side, $s>0$, at $E=1.01$ eV, while the lower reactant side barrier is at $E=0.90$ eV. The well appears to be too shallow to support a resonance state, although the barriers themselves mimic resonance dynamics.

Most important in the present work is the role of the adiabatic barriers as bottlenecks to reaction, i.e., their influence on the state-to-state reaction probabilities. Of course, the significance of adiabatic barriers in determining reaction rate constants has been explored exhaustively.[62] In some cases, the cumulative reaction probability, which is proportional to the microcanonical rate constant, exhibits visible steps as the energy passes through the bottleneck energies.[20,63] One also expects the quantized bottlenecks will influence state-to-state scattering attributes, but in a more complicated manner. Due to nonadiabatic couplings, which are largely averaged out in the cumulative reaction probability, the flux in any incoming state will be distributed over the adiabatic curves, and thus is affected by several barriers. The dynamics from this viewpoint is diagramed schematically in Fig. 8. First, the incoming flux in state (v,j) is distributed among various vibrationally adiabatic curves due to nonadiabatic couplings in the entrance channel. Then, near the transition state, each component of the flux passes over its particular adiabatic barrier. For translational energies above the barrier, the flux passes through to products, while for energies below the barrier it is largely turned back to reactants. Finally, in the exit channel the reactive flux is redistributed again among product states due to nonadiabatic coupling. The net result is that a given state-to-state reaction probability is formed from the coherent sum of amplitudes passing through all the bottlenecks. If the adiabatic picture is locally valid near the transition state, it is possible that structure in the energy dependence of the reaction probabilities may correlate with the bottleneck energies.

IV. RESULTS: EXPERIMENTAL AND THEORETICAL CROSS SECTIONS

In Fig. 9 and Table II, we present the ICSs at the two collision energies obtained from the experiment and from QM. The experimental error of $\pm 10\%$ reflects the net uncertainty in signal measurement and in the subsequent fitting and calibrations. It is seen that the experimental results and the theoretical predictions are in essentially perfect agreement for the case of ground vibrational state, $H_2(v'=0)$. As a function of final rotational quantum number, j', the $v'=0$ ICSs are seen to exhibit a strong saw-toothed behavior, where the odd j'-states have significantly larger values than the even j'-states. This, of course, is precisely the effect we anticipated from FD spin statistics. If the distributions are replotted using Boltzmann statistics (i.e., multiplying the even j'-ICS by 2 and the odd j'-ICS by 2/3), a smooth unimodal distribution is obtained as shown in Fig. 9. Focusing first on the low-energy case, $E_C=0.498$ eV, we see that significant $H_2(v'=0,j')$-product populations are observed only for $j'\leqslant 5$. Based on pure energetics, product production is possible up to $j'=7$, and thus the cutoff in the rotational distribution is dynamical in origin. For the high-energy collision, $E_C=1.200$ eV, the $v'=0$ rotational distribution broadens to include the states $j'\leqslant 9$, which again cuts off well below the energetic production threshold of $j'=12$. The low-energy case lies below the threshold for $H_2(v'=1)$, $E_C=0.552$ eV. The vibrational branching ratio at $E_C=1.200$ eV, $H_2(v'=1):H_2(v'=0)$, is found to be 0.87:0.13 in both theory and experiment. The j' distribution for $v'=1$ still shows good agreement between theory and experiment, although differences are apparent. We suspect that the small differences observed are the result of greater experimental error for the much weaker $H_2(v'=1)$ signal. While the $H_2(v'=2)$ state is energetically open at $E_C=1.200$ eV, the theoretical branching probability into this channel is extremely small, 0.001, which is well below the experimental detection limit.

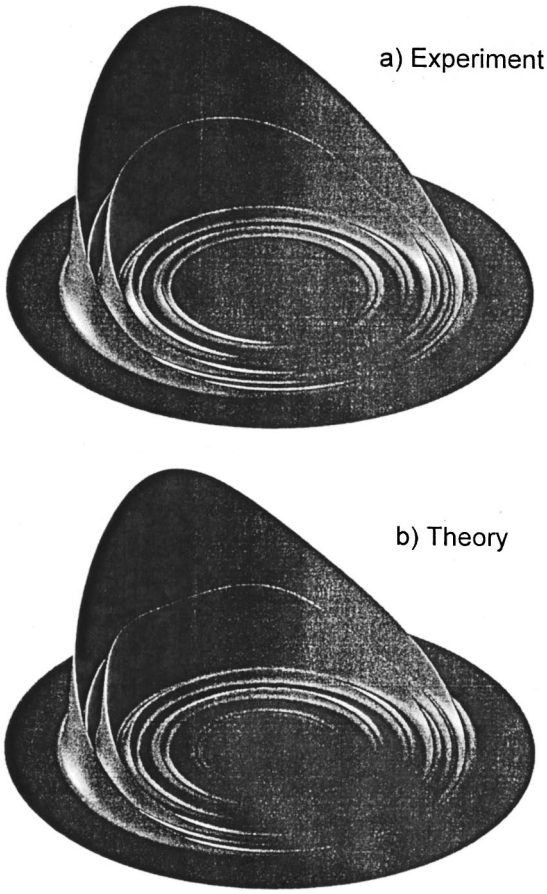

FIG. 11. The DCS for the $H+HD\rightarrow D+H_2$ reaction at $E_C=0.498$ eV plotted vs c.o.m. final velocity. The upper panel is the result of experiment, while the lower panel is QM. The individual rovibrational product states are resolved on Newton circles consistent with energy conservation; thus, the states with lower internal product energy lie on the outermost circles. Distance from the center of the diagram is scaled as velocity squared.

In Fig. 10, the rovibrationally state-specific DCS is presented versus c.o.m. scattering angle, θ, at the two energies. For the low-energy case, $E_C=0.498$ eV, the product distribution for all states is dominated by backward scattering, and shows a uniform falloff of scattering intensity as θ moves away from 180°. Theory and experiment are in good agreement for all observed product states. The higher-energy case, $E_C=1.200$ eV, yields product angular distributions that are highly structured functions of θ. Consider first the DCS for

Downloaded 12 Jul 2006 to 203.250.225.116. Redistribution subject to AIP license or copyright, see http://jcp.aip.org/jcp/copyright.jsp

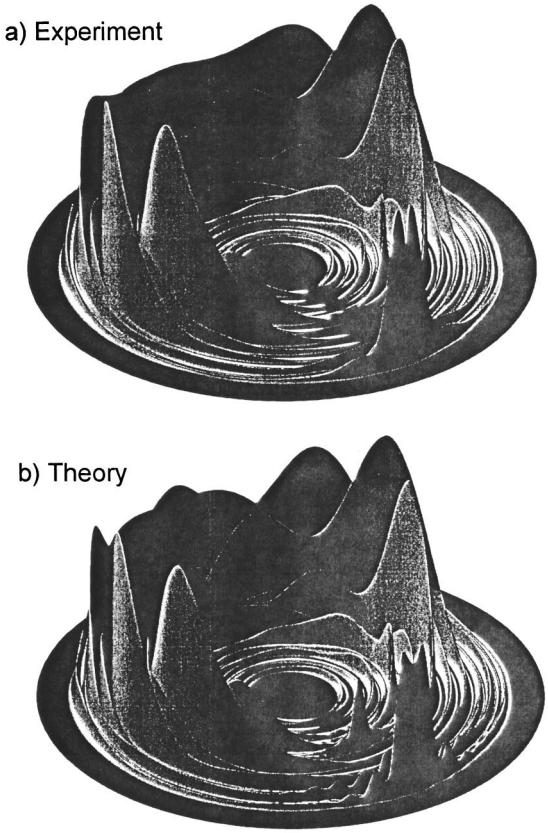

FIG. 12. Same as Fig. 11 except for $E_C = 1.200$ eV.

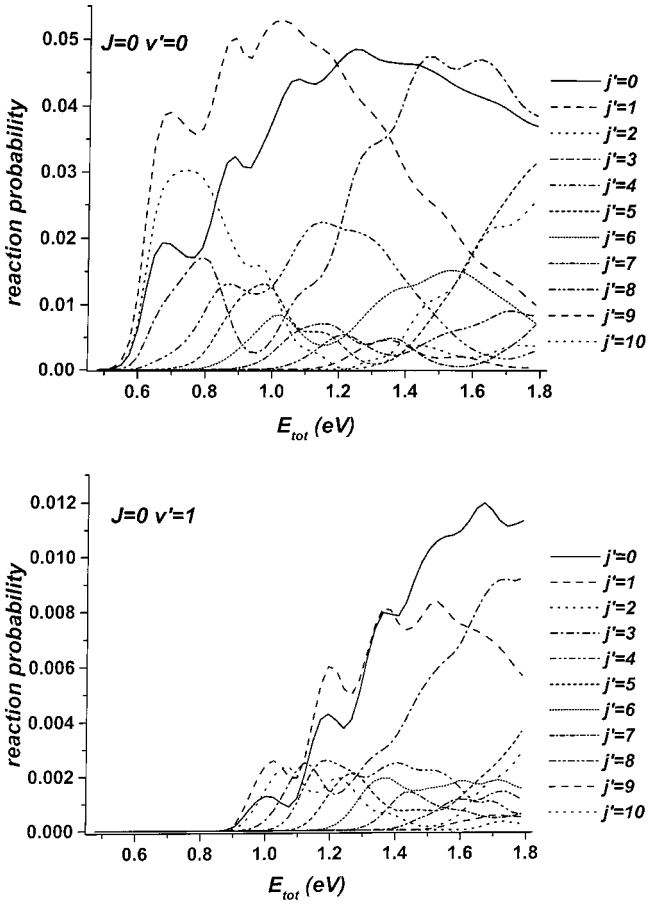

FIG. 13. The $j=0$ reaction probabilities for H+HD($v=0,j=0$)→D+H$_2$(v',j') vs total energy plotted using Boltzmann statistics to aid visualization. The upper panel is for the ground vibrational state of the product, $v'=0$, while the lower panel is for $v'=1$. The individual curves are for various rotational product states, which generally tend to higher energy with increasing j'.

the lowest product channel, $d\sigma_R(0,0\rightarrow 0,0)/d\Omega$. The DCS shows a peak in the backward direction, $\theta=180°$, with a halfwidth of about 20°. A small secondary peak is observed near $\theta=130°$. No significant signal is observed for smaller scattering angles until an intense and very narrow peak occurs in the forward direction, $\theta=0°$. The forward peak is actually about a factor of 2 higher in intensity than the backward peak. The DCS for the next two product states, i.e., H$_2$($v'=0,j'=1,2$), also clearly show the existence of the forward scattering peak. The precise peak positions shift slightly away from the forward direction for these states, however. For $j'\geqslant 3$, the forward peak completely disappears from both the experimental and QM DCSs. While the forward peak is absent for higher j' states, a higher level of structure is observed in the DCS at other scattering angles. As j' increases, the product distribution moves progressively into the sideways direction and the DCS develops oscillatory behavior. The ability of theory to reproduce the intricate angular distributions observed in experiment is impressive and reflects favorably on the accuracy of the BKMP2-PES and the scattering calculation.

The DCS for vibrationally excited product states, H$_2$($v'=1$), are shown in the bottom panel of Fig. 10. While the QM and experiment show reasonable agreement, some quantitative differences are apparent. We believe the differences are primarily due to experimental error in detecting the weak H$_2$($v'=1$) scattering signals. Nevertheless, the angular structure predicted by QM is, by and large, observed in the experiment. The most serious difference between theory and experiment is the absence of the predicted forward scattering peak in the experimental results. The QM simulations clearly predict intense forward peaks for the H$_2$($v'=1$, $j'<3$) product molecules, similar to those seen for the vibrational ground state. The origin of the disagreement, we be-

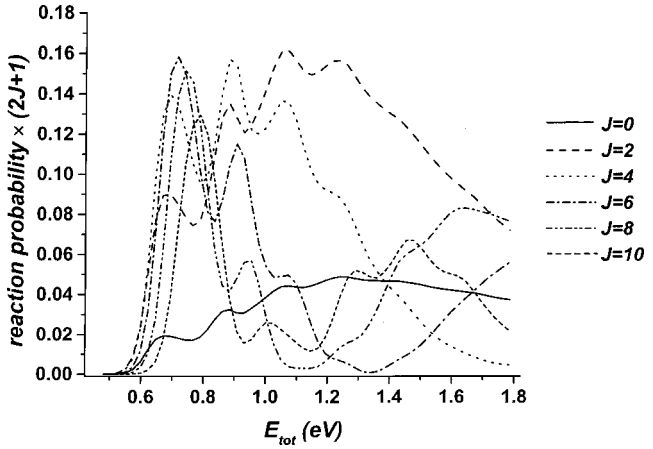

FIG. 14. The weighted state-to-state reaction probability $(2J+1)\cdot P_R^J(E;0,0\rightarrow 0,0)$ vs total energy for a number of partial waves labeled by J.

Downloaded 12 Jul 2006 to 203.250.225.116. Redistribution subject to AIP license or copyright, see http://jcp.aip.org/jcp/copyright.jsp

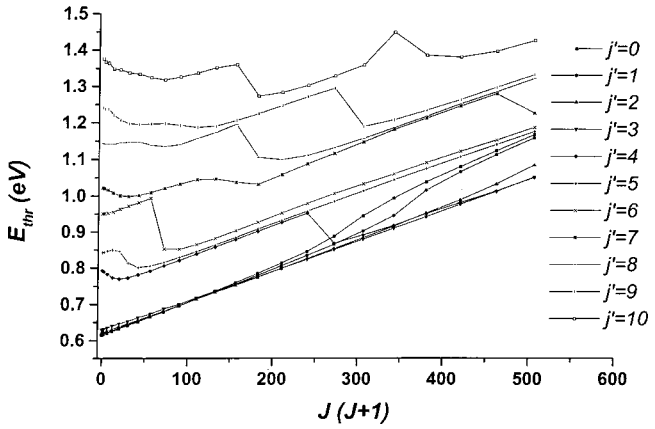

FIG. 15. The appearance thresholds vs $J(J+1)$ for the lowest 11 rotational states of H+HD $(v=0, j=0)\rightarrow$D+H_2 $(v'=0, j')$ computed from the state-to-state reaction probabilities.

lieve, is an unusually large experimental background signal at the lab angle corresponding to forward scattering in the c.o.m. frame. We conjecture that this background has obscured the observation of the forward peak, which we believe to actually exist.

An alternative method to visualize the DCS is to construct a velocity map. The DCS as a function of the c.o.m. velocity are presented in Figs. 11 and 12 for $E_C=0.498$ eV and $E_C=1.200$ eV, respectively, where the experimental results are shown in the upper panel and the results of QM are shown in the lower panel. The DCS for a given rovibrational product state, $H_2(v',j')$, lies in a Newton circle consistent with energy conservation. The outermost circles have the highest translational energy products corresponding to the lowest energy states of H_2. From the figures, one can appreciate the very strong angular variation of the DCS as a function of product translational energy. The forward scattering peaks are also displayed quite vividly.

V. ENERGY DEPENDENCE OF THE REACTIVE DYNAMICS

To obtain further insight into the dynamics of the reaction, in this section we shall present and analyze the energy dependence of the scattering results. This analysis will put into a wider perspective the previous results that were obtained at two isolated energies.

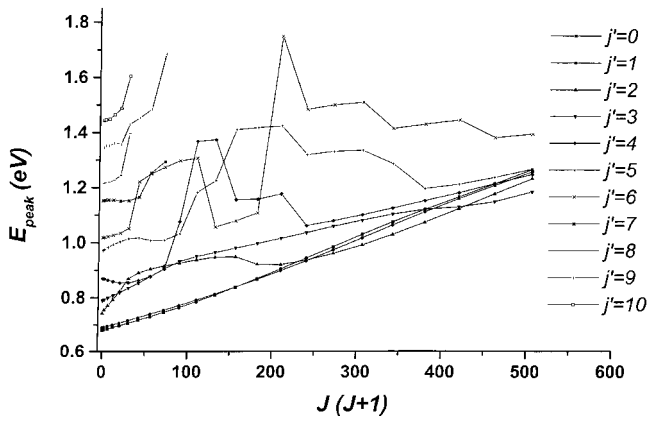

FIG. 16. The energy of the first peak of $P_R^J(E;0,0\rightarrow v'=0, j')$ plotted vs $J(J+1)$.

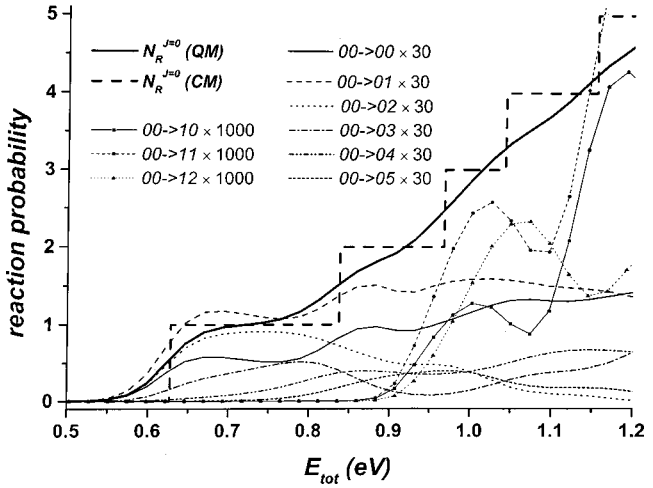

FIG. 17. The cumulative reaction probability $N_R(E,J=0)$ vs total energy. Also shown is a staircase function built from step functions located at the energies of the quantized bottlenecks. The $P_R^{J=0}(E;0,0\rightarrow v',j')$ for several states is also plotted (times a large scaling factor).

A. *J*-specific state-to-state reaction probabilities

We begin by considering the energy dependence of the state-to-state reaction probabilities computed for individual partial waves. In Fig. 13, we show reaction probabilities, $P_R^J(E;v,j\rightarrow v',j')$, from the initial state $(v,j)=(0,0)$ for the case $J=0$ of H+HD$\rightarrow$D+H_2. To make the figure easier to view, we have plotted the results using Boltzmann spin statistics, and thus the true FD results require multiplication by the factors 1/2 and 3/2; see Eq. (3.3). In the upper panel, we show $P_R^{J=0}(E;0,0\rightarrow v'=0, j')$ for $j'=0-10$, while in the lower panel the same quantities are plotted for $v'=1$. We note that some of the curves with small j' exhibit oscillation versus energy. Such oscillations are characteristic of reaction probabilities for all the isotopomers of the H+H_2 system investigated so far. It has been pointed[64] out for the H+D_2

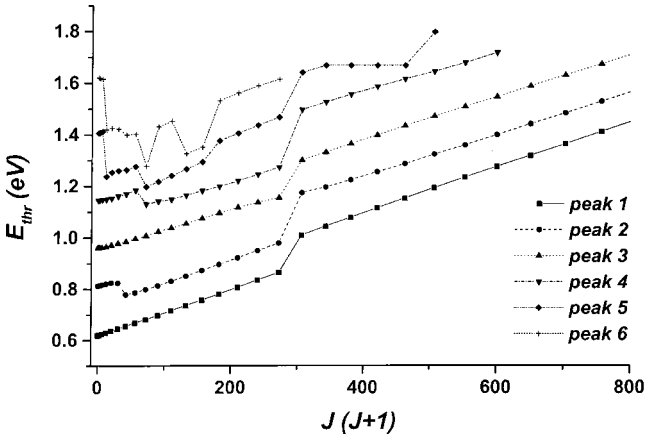

FIG. 18. The positions of the positive peaks in the derivative function of the initial state specific total reaction probability, $dN_R(E,J;v=0,j=0)/dE$, vs $J(J+1)$. The connecting lines are drawn to indicate ordering of the peaks.

Downloaded 12 Jul 2006 to 203.250.225.116. Redistribution subject to AIP license or copyright, see http://jcp.aip.org/jcp/copyright.jsp

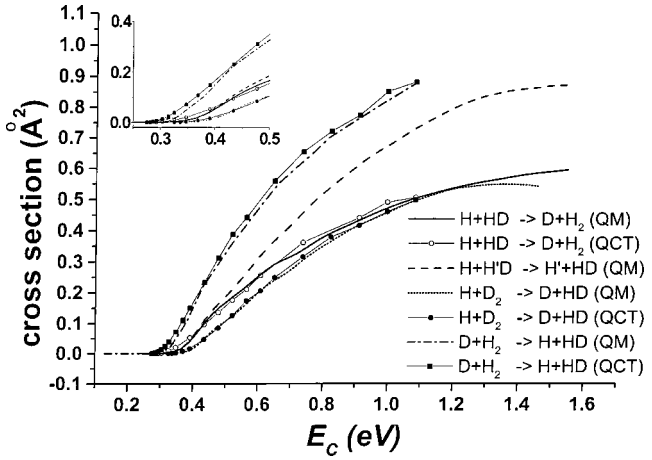

FIG. 19. Isotope effects for the excitation function, i.e., the total reactive cross section summed over final states, plotted vs total energy. QM calculations are compared with QCT results when available. The QM results for H+D_2 are from Chao and Skodje (Ref. 42), the QM for D+H_2 are from Zhang and Miller (Ref. 12), the QCT results are from Hochman-Kowal and Persky (Ref. 18). The excitation functions for homonuclear reagents are divided by 2 to compensate for the two equivalent reaction paths.

reaction that the spacing between peaks is equal to roughly twice the bending frequency at the transition state, which is also true in the present case. We also observe that the "peak" positions of the oscillations shift as a function of the final state quantum numbers, (v',j'). Each curve, $P_R^{J=0}(E;0,0\rightarrow v',j')$, exhibits a phenomological "appearance threshold," $E_{\mathrm{thr}}^{J=0}(v',j')$, which is the energy where the reaction probability first become appreciable. A reasonable definition of $E_{\mathrm{thr}}^{J=0}(v',j')$ is provided by the energy of the maximum of $dP_R^{J=0}(E;0,0\rightarrow v',j')/dE$ on the initial rise portion of the curve. Clearly, $E_{\mathrm{thr}}^{J=0}(v',j')$ lie far above the energetic thresholds for the D+$H_2(v',j')$ products and are related to the quantum bottleneck structure of the transition state.[20]

In the present study, the scattering calculations have been carried out for $J=0-35$. To show the influence of angular momentum, the quantity $(2J+1)\cdot P_R^J(E;0,0\rightarrow 0,0)$ is

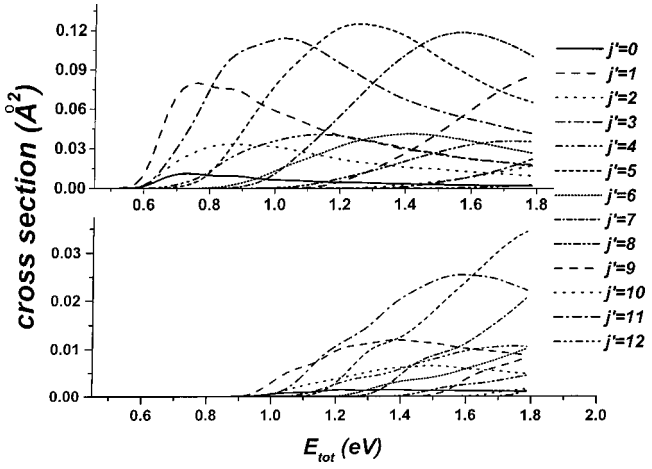

FIG. 20. The ICSs, $\sigma_R(E;0,0\rightarrow v',j')$, for H+HD→D+$H_2$ computed with FD statistics vs total energy. The upper panel shows the results for the rotational states in the $v'=0$ manifold, while the bottom panel show the results for $v'=1$.

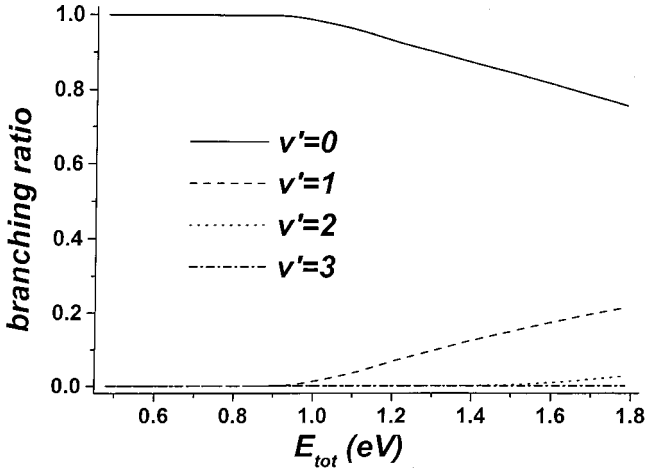

FIG. 21. The vibrational branching ratios for H+HD $(v=0,j=0)$ →D+H_2 $(v',j'=\mathrm{all})$ as a function of total energy.

plotted for a number of partial waves in Fig. 14. As J increases, $E_{\mathrm{thr}}^J(0,0)$ moves to higher values. The oscillations in the reaction probability persist and are likewise shifted to higher energy with higher J. This is qualitatively consistent with the simple J-shifting description

$$P_R^J(E;v,j\rightarrow v',j') \approx \mathrm{const}\cdot P_R^{J=0}(E-B\cdot J(J+1);v,j\rightarrow v',j'), \qquad (5.1)$$

where B is the rotation constant of the transition state. At higher J values the overall shape of the $P_R^J(E;0,0\rightarrow v',j')$ curves become quite different from the $J=0$ case, signaling at least a quantitative change in the reaction dynamics for the centrifugally modified potential.

To provide a more quantitative analysis of the influence of J on the reaction probability, in Fig. 15 we plot the threshold energies $E_{\mathrm{thr}}^J(v',j')$ versus $J(J+1)$ for a number of final

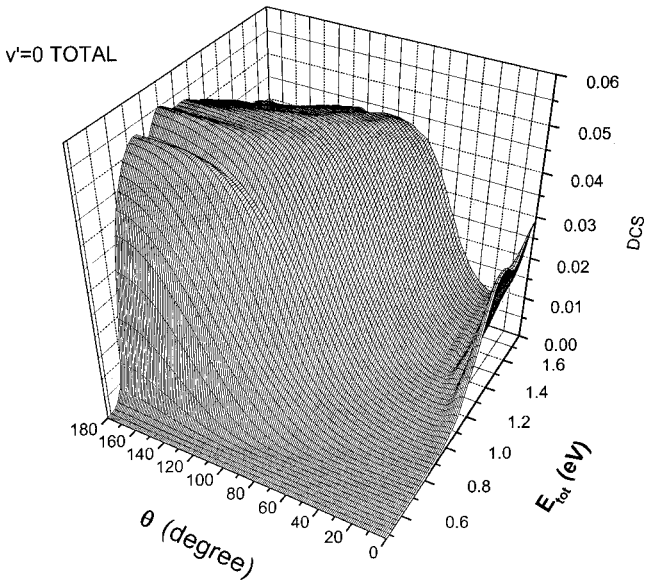

FIG. 22. The total reactive DCS in $Å^2/sr$ for H+HD $(v=0,j=0)$ →D+H_2 $(v',j'=\mathrm{all})$ as a function of total energy and c.o.m. scattering angle.

Downloaded 12 Jul 2006 to 203.250.225.116. Redistribution subject to AIP license or copyright, see http://jcp.aip.org/jcp/copyright.jsp

states of the $H+HD(0,0)\rightarrow D+H_2(v'=0,j')$ reaction. As is expected, the thresholds generally evolve to higher energy as J increases. However, occasionally the peaks of $dP_R^{J=0}(E;0,0\rightarrow v',j')/dE$ will evolve into shoulders as J is varied, which leads to the abrupt jumps in the position of the ''first peak'' that are apparent in the plot. The first several product states, corresponding to $j'=0-3$, exhibit nearly equal threshold energies up to $J\sim 15$. For $J<15$, the dependence of $E_{\mathrm{thr}}^J(0,0)$ on $J(J+1)$ is roughly linear, with a B constant of 7.2 cm^{-1} and an intercept at 0.62 eV. The simplest interpretation of this result is that the threshold for production of the first four rotational states of H_2 are controlled by a single quantized bottleneck state with a rotation constant of 7.2 cm^{-1}, i.e., clearly the $(0,0^0)$ state. The higher rotational product states show more complicated threshold behavior, and nonlinear dependence on $J(J+1)$ is clearly manifested. Nevertheless, the results appear to suggest the existence of at least two other quantized bottlenecks lying approximately 0.2 and 0.4 eV above the lowest bottleneck, corresponding to bend-excited states.

We have also investigated the J dependence of the oscillatory structure of exhibited by the state-to-state reaction probabilities. In particular, the peak positions of the oscillations were followed as functions of J. In Fig. 16, the position of the first peak in $P_R^J(E;0,0\rightarrow v'=0,\ j'=0-10)$ is plotted versus $J(J+1)$. From the standpoint of the simple J shifting prescription, the results are seen to be rather dismal. The two lowest product states, $j'=0$ and 1, show smooth monotonic growth with J, although the curves exhibit enough nonlinearity to make the assignment of a B constant rather arbitrary. The higher-lying j'-product states show an erratic J dependence which defies any simple interpretation. The higher peaks of the oscillating reaction probability likewise exhibit complicated and nonlinear behavior versus

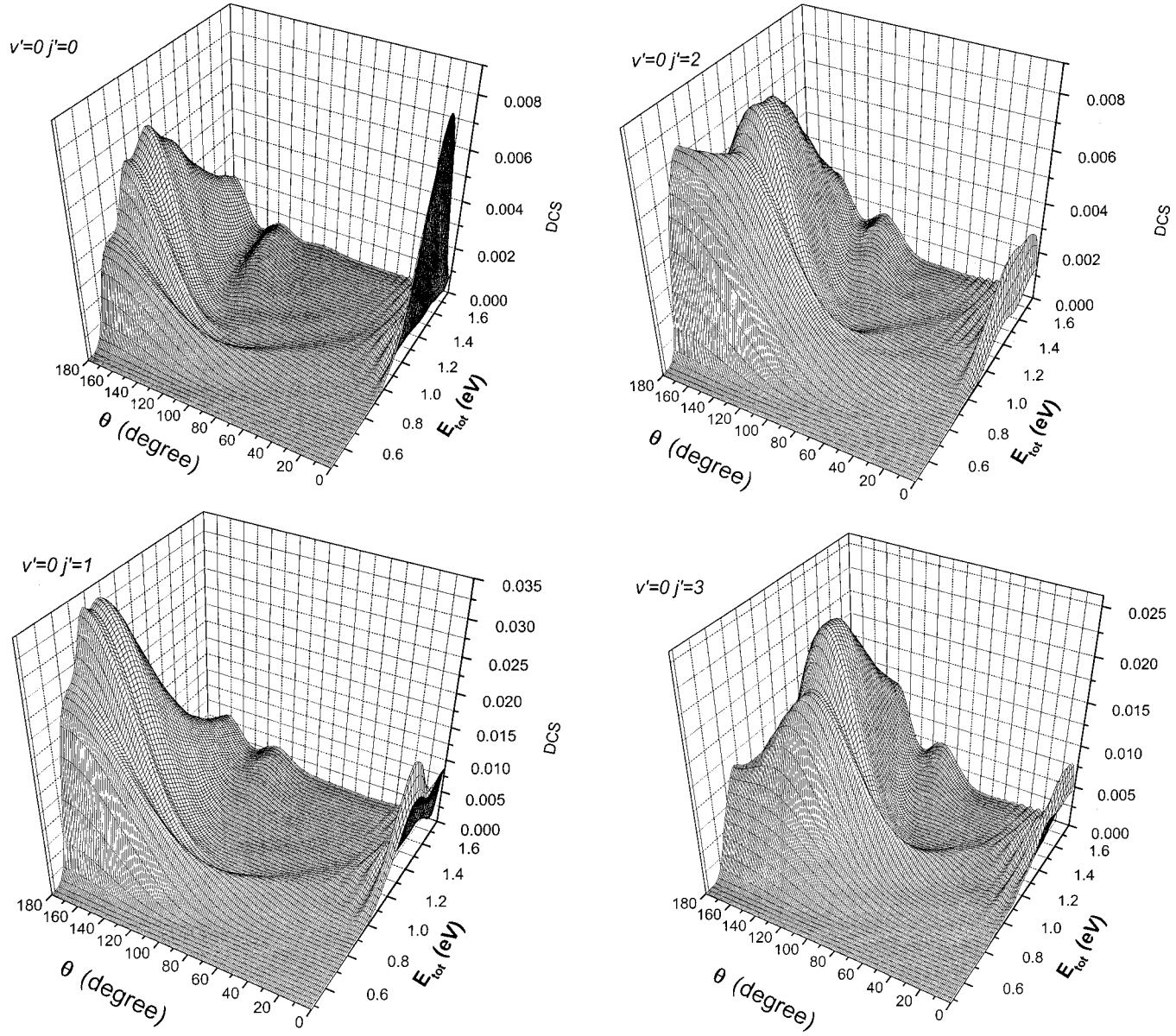

FIG. 23. The state-to-state DCS in $\mathrm{Å}^2/sr$ for $H+HD(v=0,j=0)D+H_2(v'=0,j')$ for a number of final rotational states as a function of total energy and c.o.m. scattering angle.

Downloaded 12 Jul 2006 to 203.250.225.116. Redistribution subject to AIP license or copyright, see http://jcp.aip.org/jcp/copyright.jsp

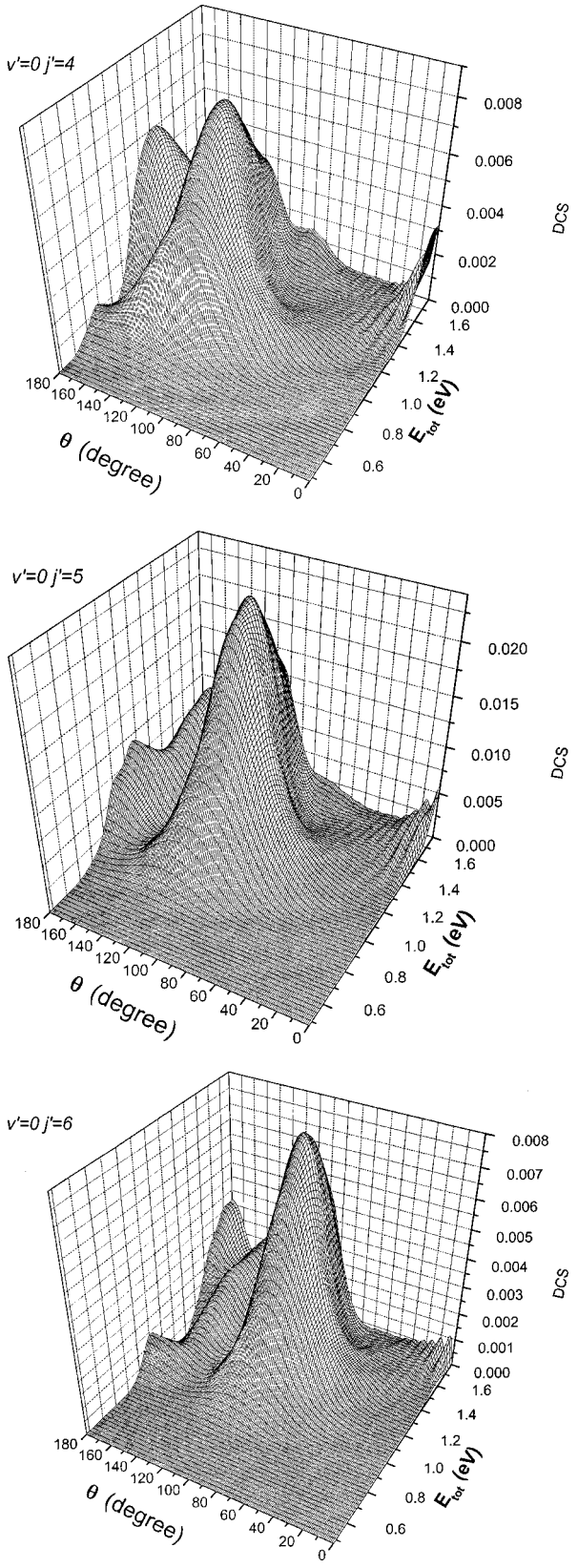

FIG. 23. (*Continued.*)

$J(J+1)$. The results seem inconsistent with the view that the oscillations in the reaction probabilities can be directly tied to the existence of conventional Breit–Wigner resonances lying at energies near the peaks. If such a resonance picture held true, one would naively expect the peak positions should evolve linearly with $J(J+1)$, with a B constant consistent with the resonance state wave function. To use the resonance concept to classify the oscillations would require an explicit analysis of the interference between Breit–Wigner pole terms and the background scattering amplitude. An alternative method to diagnose the existence of resonances is provided by the computation of the scattering time delay. However, we have found the results of such an analysis to be equally ambiguous for the oscillations in the reaction probability.[21]

It is useful to compare the structure of $P_R^J(E;v,j\rightarrow v',j')$ with the cumulative reaction probability, $N_R(E,J)$, which is the sum of $P_R^J(E;v,j\rightarrow v',j')$ over all open reactant and product states at energy E. In Fig. 17, $N_R(E,J)$ is shown for the case $J=0$, along with a few of the individual state-to-state probabilities from which it is composed. For reference, we have also plotted the staircase function

$$F_R(E)=\sum_{\mathbf{n}}\ \theta(E-E_{QM}(\mathbf{n})), \tag{5.2}$$

which is simply the sum of step functions associated with each quantized bottleneck taken from the data of Chatfield *et al.*[20] Several of the reaction steps are visible and $N_R(E,J=0)$ shows a monotonic increase. Absent are any dips or bumps that might be tied to conventional resonance behavior. It seems clear that the oscillations of the reaction probability, which occur ''out of phase'' for the various $(v,j\rightarrow v',j')$ reactive transitions, combine to form the reactive steps. As demonstrated convincingly by the work of Chatfield *et al.*,[20] the steps are correlated to the energies of the adiabatic barriers, which we have also verified in the present case. Thus, we are led to suspect that the oscillations in $P_R^J(E;v,j\rightarrow v',j')$ over the present energy range are the by-product of the opening of new reactive pathways, i.e., thresholds, as diagramed schematically in Fig. 8, as opposed to conventional resonance phenomenon. Since we did not compute the full S matrix for $J\neq 0$, we cannot directly investigate the J shifting of $N_R(E,J)$. However, we can compute the initial-state-selected reaction probability, $N_R(E,J;v=0,j=0)$, which is the total reaction probability from initial state $(v,j)=(0,0)$. This quantity has been shown[20] to be sensitive to the location of bottleneck energies via positive peaks in the derivative function, $dN_R(E,J;v=0,j=0)/dE$. The peak positions of the derivative versus $J(J+1)$ are plotted in Fig. 18. The results are similar to the J shifting of the appearance thresholds for $P_R^{J=0}(E;0,0\rightarrow v',j')$, Fig. 15, but are much ''cleaner'' due to the suppression of some of the nonadiabatic coupling. The peak positions are found to correlate to the adiabatic barrier energies using the simplest prescription, $V_{\max}(\mathbf{n},J)=V_{\max}(\mathbf{n},J=0)+\hbar^2J(J+1)/2I^{\ddagger}$. (Some of the abrupt jumps in the peak positions are due to the breaking the restriction of $v_{\text{bend}}=$even when $J\neq 0$.) The simple J dependence of the peaks tends to reinforce the view that the reaction steps, and the closely related appearance thresholds, are both manifestations of quantum bottleneck effects.

Downloaded 12 Jul 2006 to 203.250.225.116. Redistribution subject to AIP license or copyright, see http://jcp.aip.org/jcp/copyright.jsp

B. Integral cross sections

To model scattering observables, the results for the individual partial waves should be combined to produce the ICS and DCS. In Fig. 19, the total reactive integral cross section (the excitation function) for the reaction $H+HD(v'=0, j'=0) \rightarrow D+H_2(v'=\text{all}, j'=\text{all})$ is plotted versus energy. For comparison purposes, we have also included the QCT results of Hochman-Kowal *et al.*,[18] carried out on the DMBE-PES. Not suprisingly, the detailed structure that occurs for single partial waves is largely suppressed in the highly averaged excitation function. As observed previously for other isotopomers of the $H+H_2$ system, the QCT simulations give quite good agreement with the full quantum-mechanical results except, near threshold, where tunneling is important. Also included in Fig. 19 is the excitation function for the unobservable reaction channel, $H+H'D \rightarrow H'+HD$, as well as for the two other isotopomers, $D+H_2 \rightarrow H+HD$ and $H+D_2 \rightarrow D+HD$. For the later two reactions, the excitation functions are divided by 2 in order to account for the two equivalent reaction sites. The excitation function for $H+H'D \rightarrow H'+HD$, is seen to be larger than $H+HD \rightarrow D+H_2$. This is consistent with the cone of acceptance argument of Levine.[65]

More pertinent to the comparison to experimental results are the final state-selective integral cross sections, $\sigma_R(E;0,0 \rightarrow v',j')$. These quantities are plotted in Fig. 20 versus total energy for the final states $v'=0,1$ and $j'=0-12$. As with the state-specific reaction probabilities, $\sigma_R(E;0,0 \rightarrow v',j')$ exhibit appearance thresholds for the production of specific final states. Because of summing over J, the thresholds do not appear as sharp and tend to be shifted to somewhat higher energies compared to those for $P_R(E;0,0 \rightarrow v',j')$. The thresholds, defined as before using the peaks in the derivative of $d\sigma_R(E;0,0 \rightarrow v',j')/dE$, are roughly equal for $j'=0-3$, and for the larger j' states are shifted progressively higher in energy. The spin statistics factors have a dramatic influence on final rotational distribution, with the $j'=$ odd H_2 products produced in greater abundance

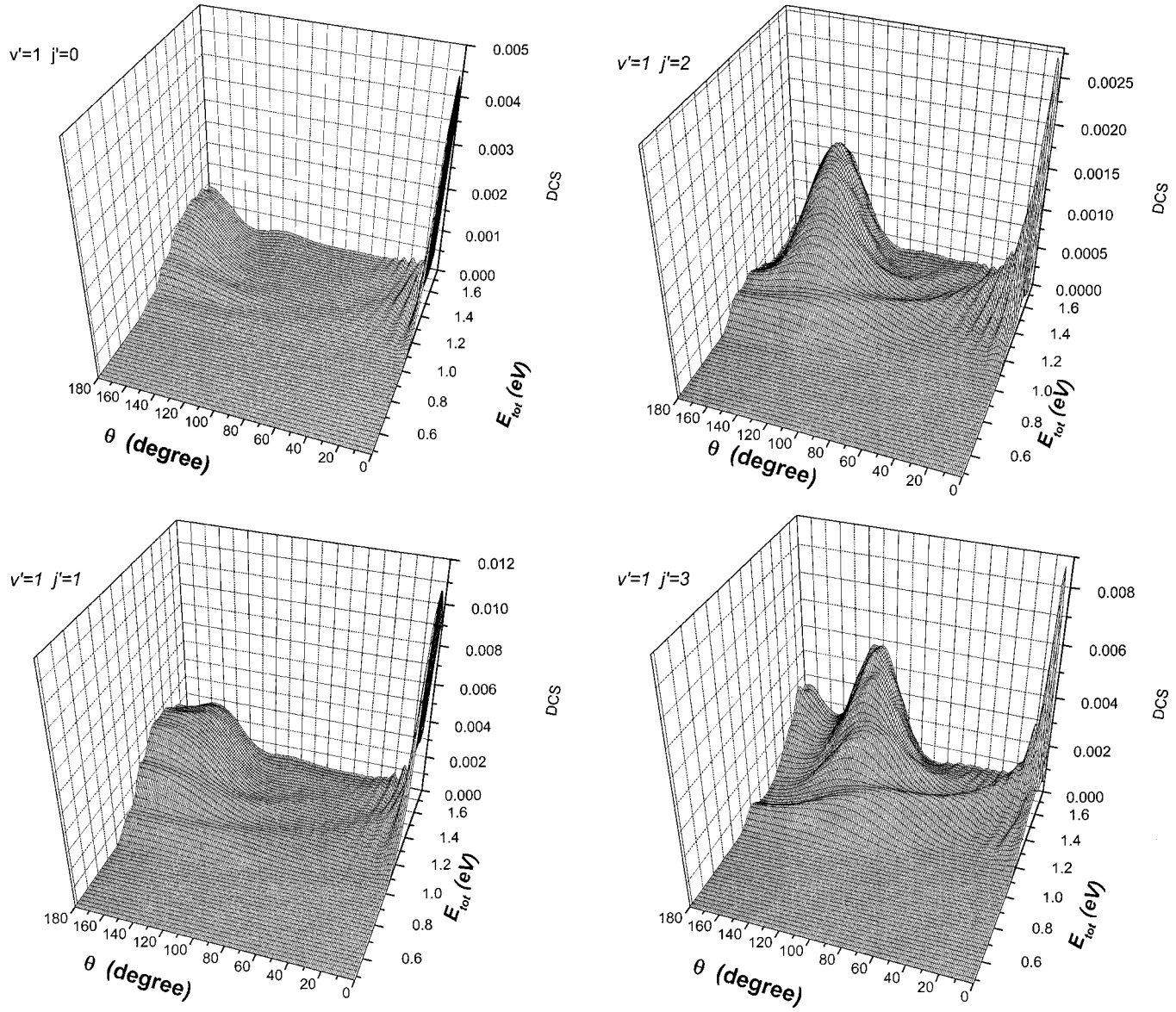

FIG. 24. Same as Fig. 23 except for $v'=1$ product states.

Downloaded 12 Jul 2006 to 203.250.225.116. Redistribution subject to AIP license or copyright, see http://jcp.aip.org/jcp/copyright.jsp

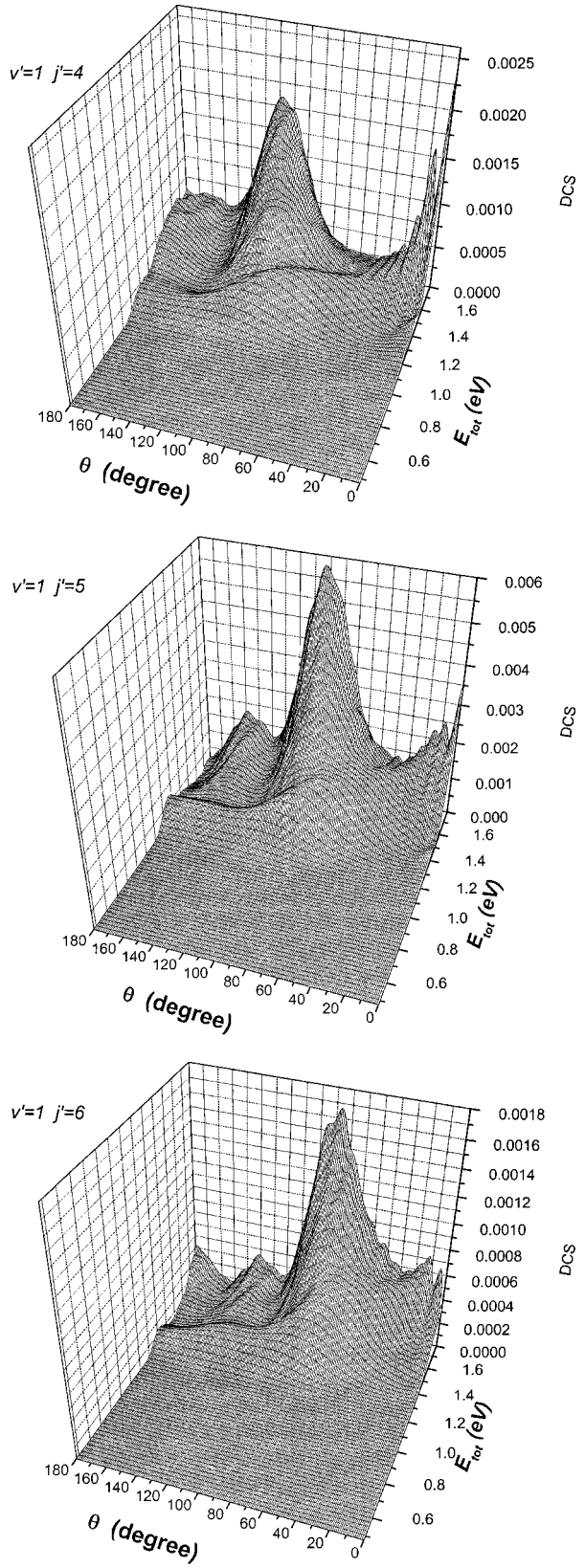

FIG. 24. (*Continued.*)

than the $j'=$even products. The 3:1 statistical weighting of *ortho:para* states is reflected to surprising accuracy in the final product distributions of rotational states. Specifically, the ratio

$$F(E,v')=\frac{\Sigma_{j'}^{\text{odd}}\sigma_R(E;0,0\rightarrow v',j')}{\Sigma_{j'}^{\text{even}}\sigma_R(E;0,0\rightarrow v',j')}, \tag{5.3}$$

within each vibrational manifold is found to equal 3 to ~0.1% accuracy even when as few as four rotational states dominate the distribution (>99%).

The oscillations observed in the state-to-state reaction probabilities are largely washed out when the ICSs are computed. However, one does see rather faint traces of oscillation for several of the product states, particularly the $v'=1$ manifold. We note that the oscillation of the ICSs seen here for the H+HD→D+H$_2$ isotopomer is decidedly smaller than those for the H+D$_2$→D+HD reaction studied previously.[42]

The vibrational branching ratios for H+HD→D+H$_2$ are obtained by summing the ICSs for all open rotational states. As seen in Fig. 21, the vibrationally excited product states appear slightly above the energetic thresholds of H$_2$(v',$j'=0$) and exhibit a smooth structureless evolution as function of total energy.

C. Differential cross sections

The total reactive DCS for H+HD→D+H$_2$, obtained by summing over all final product states of H$_2$($v'=0$), from the initial state HD($v=0$,$j=0$) is plotted over the full energy range in Fig. 22. The DCS shows a plateau in the backward hemisphere, which grows further into the sideways direction with increasing energy. A discernible oscillation is present in the backward direction, $\theta=180°$. Above about $E=1.0$ eV, a narrow forward scattering peak is observed.

The individual state-to-state DCSs reveal more angular structures than the total reactive DCS. In Figs. 23 and 24, the DCSs for a number of representative product states are shown. In the first panel of Fig. 23, $d\sigma_R(E;0,0\rightarrow 0,0)/d\Omega$ is plotted versus scattering angle and energy. At low energy, the products are peaked in the backward direction, $\theta=180°$, consistent with the usual rebound mechanism in a system with a collinear reaction path. Weak oscillations are observed in the DCS for $\theta=180°$. A ridge structure, similar to that seen earlier by Zhang and Miller[12] for H+H$_2$, emerges from the lowest "peak" in the oscillation as part of the product distribution moves smoothly to the sideways direction. This ridge is clearly associated with the J shifting of the lowest adiabatic barrier and not with conventional resonance phenomena. For energies $E>1.0$ eV, a strong and very narrow forward scattering peak is observed. While the forward peak in $d\sigma_R(E;0,0\rightarrow 0,0)/d\Omega$ is actually higher than the backward peak, the backward scattering still dominates the reactive flux due to the sin θ weighting factor in the definition of solid angle, $d\Omega$.

The DCSs for rotationally excited products, D+H$_2$($v'=0$, $j'>0$), shown in Fig. 23, show a progressive shift toward sideways scattering as j' increases, consistent with angular momentum constraints. Furthermore, large angular oscillations develop and proliferate with higher j'. The forward peak in $d\sigma_R(E;0,0\rightarrow 0,j')/d\Omega$ is seen to persist for $j'=0-5$, although it shifts to higher energy as j' increases and the peak position moves slightly away from $\theta=0°$ for $j'>0$. This behavior is consistent with that of the Wigner

Downloaded 12 Jul 2006 to 203.250.225.116. Redistribution subject to AIP license or copyright, see http://jcp.aip.org/jcp/copyright.jsp

functions, $d^{J}_{kk'}(\theta)$, for high J. It is entirely possible that the forward peak for $j'>5$ may continue to exist, but at higher energies than considered in the present calculations.

The angular oscillations in the DCSs can be traced back, at least partly, to the contributions of specific helicity states. As an example, the separate helicity contributions, $d\sigma_R(E;0,0,k=0\rightarrow 0, j', k')/d\Omega$, are plotted in Fig. 25 for the case $H+HD(v=0, j=0)\rightarrow D+H_2(v'=0, j'=6)$. It is seen that each of the angular peaks in $d\sigma_R(E;0,0\rightarrow 0,6)/d\Omega$ is dominated by much more pronounced peaks occurring in helicity specific DCSs.

The DCSs for the vibrationally excited product state, $H_2(v'=1, j')$, are seen in Fig. 24 to show some similarities to the $H_2(v'=0, j')$ case, although there is an overall shift to higher energy. Significantly, the forward peak observed for $H_2(v'=0, j'=0-2)$ is also seen for the vibrationally excited product.

D. Analysis of the forward scattering peak

Perhaps the single most dramatic observation in the present study is that of an extremely narrow forward peak in the reactive DCSs for $H+HD(0,0)\rightarrow D+H_2(v'=0-1, j'=0-2)$. In a subsequent publication,[21] we shall examine the dynamics associated with this peak in greater depth. Here, we shall present a preliminary characterization of the peak.

We begin by describing the observable characteristics of the forward peak at the experimental energy $E_C=1.200$ eV. The DCS for the $H_2(0,0)$ product, computed from QM on a fine angular grid, is peaked at $\theta=0°$ with a full width at half maximum of merely 2.5°. For the $H_2(0,1)$ and $H_2(0,2)$ product states, the peak shifts slightly to 3.55° and 4.29°, with half widths at half maxima of 3.62° and 3.26°. For the vibrationally excited products $H_2(1,0)$, $H_2(1,1)$, and $H_2(1,2)$, the peaks positions are 0°, 0°, and 4.6° and widths are 2.3°, 3.5°,

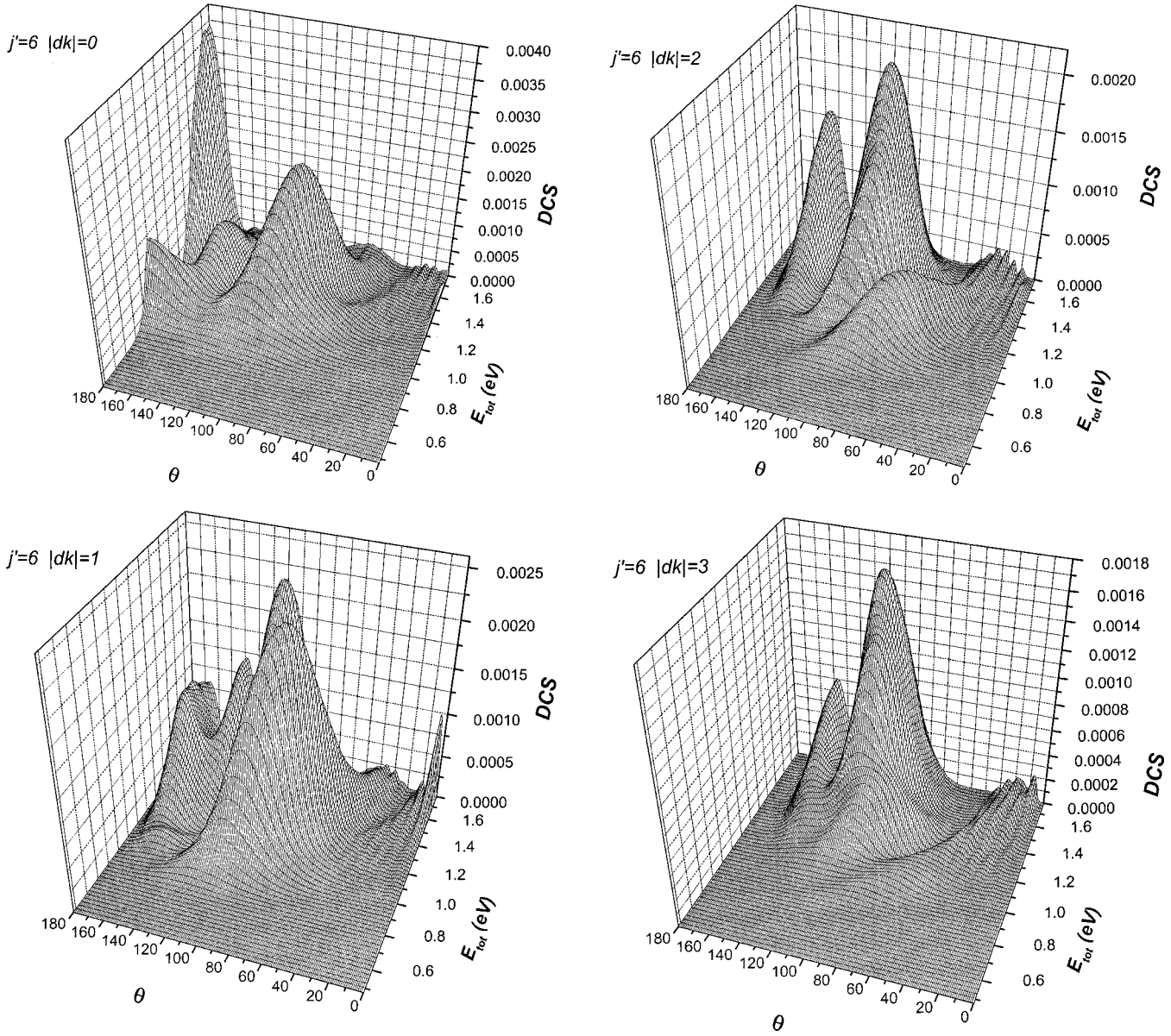

FIG. 25. Contributions of separate helicity states to the DCS for $H+HD(v=0, j=0)\rightarrow D+H_2(v'=0, j'=6)$. Plotted is $d\sigma_R(E;0,0,0\rightarrow v'=0, j'=6, k')/d\Omega$ vs c.o.m. scattering angle and total energy.

Downloaded 12 Jul 2006 to 203.250.225.116. Redistribution subject to AIP license or copyright, see http://jcp.aip.org/jcp/copyright.jsp

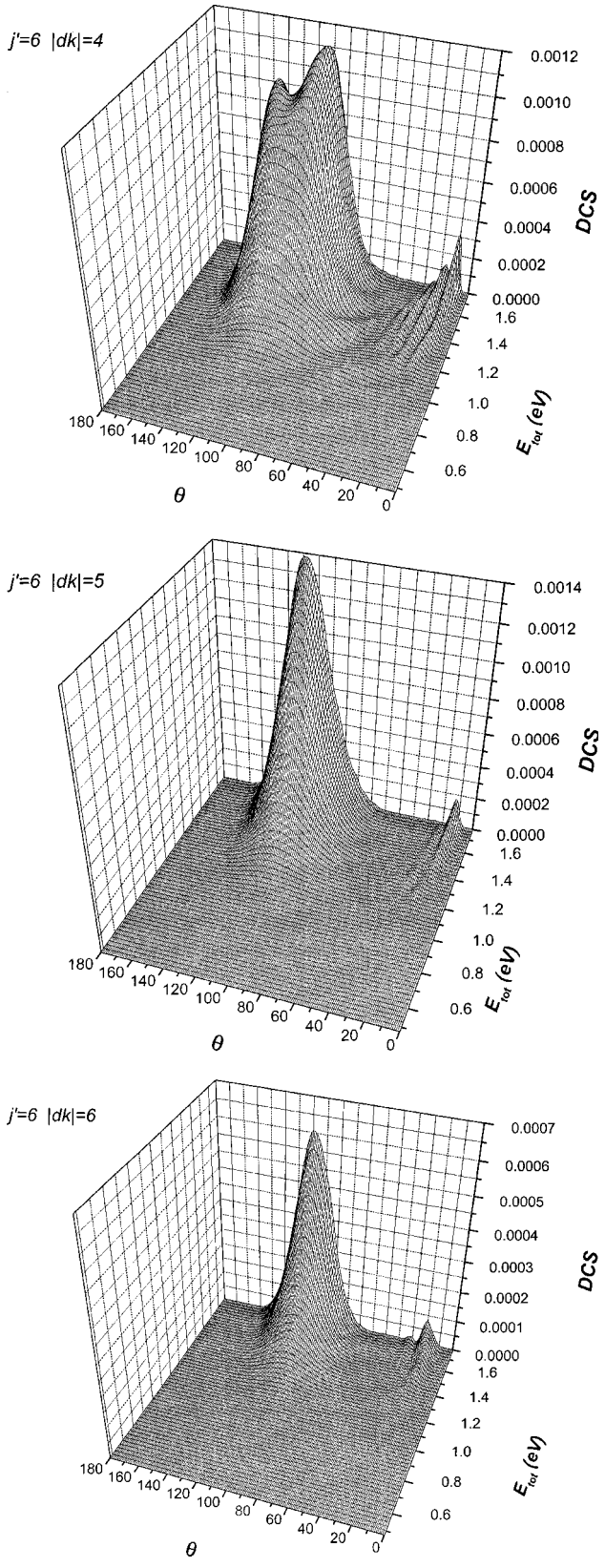

FIG. 25. (*Continued.*)

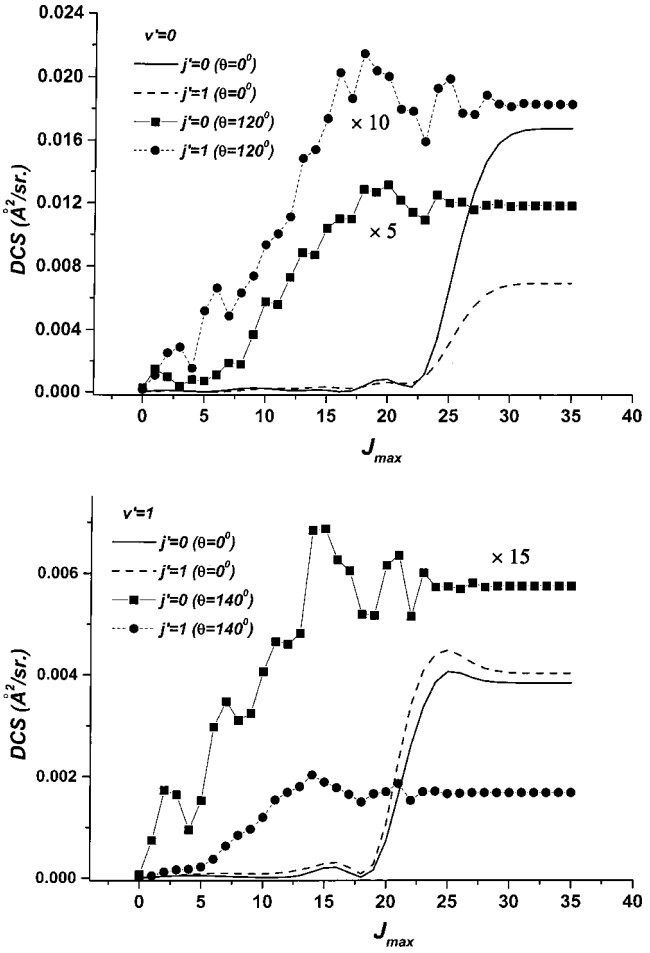

FIG. 26. The state-specific angular opacity function vs J at $E_C = 1.200$ eV. The upper panel shows the result for $(v',j')=(0,0)$ and $(0,1)$ in the forward direction, $\theta=0°$, and a sideways direction, $\theta=120°$. The sideways scattering results are multiplied by a constant to aid visualization. The lower panel is the same except for final states $(v',j')=(1,0)$ and $(1,1)$ and $\theta=140°$.

and 3.4°. The rovibrational product distribution within the forward peak is found to be rotationally cold and vibrationally hot. By averaging the DCS over the narrow interval $\theta=[0–5°]$, it is found that $\langle j' \rangle_{\theta=0}=1.3$ and $\langle E'_{\rm vib}\text{-}E_{H_2}(v'=0, j'=0)\rangle_{\theta=0}=1137\ {\rm cm}^{-1}$. These numbers can be contrasted with the ICS results that average over all scattering angles over all angles of $\langle j' \rangle_{\rm all}=5.3$ and $\langle E'_{\rm vib}\text{-}E_{H_2}(v'=0, j'=0)\rangle_{\rm all}=556\ {\rm cm}^{-1}$. While some of the difference between the forward peak and the other scattering angles may result simply from angular momentum constraints, the magnitude of the differences suggests that the details of the reaction dynamics proceeding in the forward direction may differ from that going into the remaining angles.

It has been noted previously[32,45,54] that forward scattering peaks in atom+diatom reactions are often the result of collisions occurring at high impact parameters. Since the initial rotational state of HD is $j=0$, this would suggest that high values of $J(=L)$ may play an important role. To quantify this idea, we compute the state- and angle-specific integrated opacity function,[54] $d\sigma_{J_{\rm max}}(0,0\rightarrow v', j')/d\Omega$. This quantity is simply the state-to-state DCS at fixed E (using Boltzmann statistics to aid visualization) computed using a partial sum of J-states where $j \leqslant J_{\rm max}$, i.e.,

Downloaded 12 Jul 2006 to 203.250.225.116. Redistribution subject to AIP license or copyright, see http://jcp.aip.org/jcp/copyright.jsp

$$\frac{d\sigma_{J_{\max}}(0,0\rightarrow v',j')}{d\Omega} = \frac{1}{4k_{vj}^2}\sum_{k'}\left|\sum_{J=0}^{J_{\max}}(2J+1)\cdot d^{J}_{o,k'}(\pi-\theta)\cdot S_B^{\alpha\rightarrow\gamma}(0,0,0\rightarrow v',j',k')\right|^2. \quad (5.4)$$

In Fig. 26, we fix the scattering angle at the forward peak and $E_C=1.200$ eV, and compute $d\sigma_{J_{\max}}(0,0\rightarrow v'=0,\ j'=0,1)/d\Omega$ and $d\sigma_{J_{\max}}(0,0\rightarrow v'=1,\ j'=0,1)/d\Omega$; for comparison we also show the result computed for sideways scattering, $\theta=120°$ and $\theta=140°$. It is seen from the figure that the forward peak is dominantly due to the contributions of several partial waves near $j_{\max}=25$ for $v'=0$ and $j_{\max}=21$ for $v'=1$. On the other hand, for sideways scattering (and other arbitrary scattering angles) a much larger range of angular momenta contributes. At $J=L=25$ and $E_C=1.200$ eV, the classical impact parameter relative to the HD c.o.m. is 2.3 bohr, corresponding to a glancing-type collision as opposed to the head-on type collision envisioned for low L collisions.

In light of the preceding discussion, the analysis of the forward scattering peak can focus on the dynamics of high impact parameter scattering. In a subsequent publication, we shall find that in fact trapping occurs near the quantized bottleneck for the centrifugally modified Hamiltonian.

VI. CONCLUSIONS

In this work, we have presented the first detailed experimental and QM study of the reaction dynamics of $H+HD\rightarrow D+H_2$. The overall conclusion of the work is that the scattering observables for theory and experiment are in quantitative agreement at the energies considered. On one level, this agreement serves as a check for systematic error in the experiment and for inaccuracy in the PES or the dynamics calculations. Perhaps the most significant conclusion along this line is that apparently the GP does not play a major role in the dynamics for the energies considered in the present experiment. However, caution should be exercised in this matter since the GP may in fact have a much larger influence at other collisions not considered here. On a deeper level, the theory and experiment provided mutual guidance. For example, the forward peak was originally predicted based on the QM calculations. This motivated an experimental search on a fine angular grid to detect the peak.

The ICSs and DCSs have been computed based on converged scattering calculations for 56 total energies between 0.48 and 1.79 eV to allow an analysis of the reaction dynamics. A number of the individual state-to-state reaction probabilities (for fixed J) exhibit oscillation with energy that we have come to expect in all the isotopomers of the $H+H_2$ family. In the present reaction, unlike the case of $H+D_2$,[42] the oscillations are largely washed out in the cross sections. The strongest remnants of the oscillation remain in the DCS near backward scattering. Potential experimental observation of the oscillation, using a tunable energy beam source, should have the best chance of success by focusing on the DCS in the backward direction.

Spin statistics was found to play a major role in determining the rotational product distribution. When the state-resolved ICSs are calculated using Boltzmann statistics, the rotational distribution is broad and unimodal. The inclusion of FD-spin statistics through postantisymmetrization induces a pronounced saw-toothed distribution where the odd rotational states are three times more highly populated than the even states. The previous results of Zare and co-workers[49] for $H+HI\rightarrow I+H_2$, which demonstrated a similar saw-toothed rotational distribution, suggest that this effect should be expected for $A+AB\rightarrow B+A_2$ type reactions.

While the state-to-state reaction probabilities and, to a much smaller extent, the ICS and DCS do exhibit structure as a function of collision energy, it is difficult to make a case for the influence of reactive resonances. The adiabatic potential wells for $v_{ss}\leqslant 1$ are too shallow to support Feshbach resonances, which do not appear until $E>2$ eV even for the more favorable collinear (two-dimensional) reaction.[66] The inclusion of the bend and also the centrifugal potential for higher J, tend to make the wells even shallower. Thus, any contributing ''resonance'' would have to be a barrier-type state,[66,67] which corresponds to time delay near a barrier maximum. While barrier states can appear vividly as assignable peaks in transition state spectra, their utility in interpreting scattering data as conventional resonance phenomena is much more problematic. The core of the problem is of course that the reaction probabilities for barriers exhibit threshold behavior rather than Lorentzian peaks. This leads to a host of difficulties in separating the pole contribution to the S matrix from that of the background, which is changing rapidly versus E. While it seems clear that the appearance thresholds and oscillations in $P_R^J(E;v,j\rightarrow v',j')$ are tied to the adiabatic barriers, and hence to barrier states *per se*, this is not equivalent to saying that they should be interpreted as ''resonance phenomena.'' Perhaps a more promising direction for the resonance view is in the analysis of the forward scattering peak. In a subsequent paper we shall investigate more carefully the dynamics associated with this feature.

ACKNOWLEDGMENTS

The authors are grateful to Kopin Liu for many insightful discussions. This work was supported by the National Science Foundation and the National Research Council of Taiwan. R.T.S. and S.D.C. acknowledge the support of the Institute for Molecular Science.

[1] J. J. Valentini and D. L. Phillips, in *Advances in Gas Phase Photochemistry*, edited by M. N. R. Ashfold and J. E. Baggot (Royal Society of Chemistry, London, 1989), Vol. 2, p. 1.
[2] H. Buchenau, J. P. Toennies, J. Arnold, and J. Wolfrum, Ber. Bunsenges. Phys. Chem. **94**, 1231 (1990).
[3] W. H. Miller, Annu. Rev. Phys. Chem. **41**, 245 (1990).
[4] L. Schnieder, K. Seekamp-Rahn, J. Borkowski, E. Wrede, and K. H. Welge, Science **269**, 207 (1995); L. Schnieder, K. Seekamp-Rahn, E. Wrede, and K. H. Welge, J. Chem. Phys. **107**, 6175 (1997); E. Wrede, L. Schnieder, K. H. Welge, F. J. Aoiz, and L. Bañares, *ibid.* **106**, 7862 (1996).
[5] T. N. Kitsopoulos, M. A. Buntine, D. P. Baldwin, R. N. Zare, and D. W. Chandler, Science **260**, 1605 (1993).

Downloaded 12 Jul 2006 to 203.250.225.116. Redistribution subject to AIP license or copyright, see http://jcp.aip.org/jcp/copyright.jsp

[6] K. Liu, Annu. Rev. Phys. Chem. **52**, 139 (2001), and references therein.
[7] F. Fernandez-Alonso, B. D. Bean, and R. N. Zare, J. Chem. Phys. **111**, 1022 (1999); **111**, 2490 (1999); F. Fernandez-Alonso, B. D. Bean, R. N. Zare, F. J. Aoiz, L. Bañares, and J. F. Castillo, *ibid.* **115**, 4534 (2001).
[8] S. A. Buntin, C. F. Giese, and W. R. Gentry, J. Chem. Phys. **87**, 1443 (1987).
[9] P. Casavecchia, Rep. Prog. Phys. **63**, 355 (2000), and references therein.
[10] A. I. Boothroyd, W. J. Keogh, P. G. Martin, and M. R. Peterson, J. Chem. Phys. **104**, 7139 (1996).
[11] Y.-S. M. Yu, A. Kuppermann, and J. B. Anderson, Phys. Chem. Chem. Phys. **1**, 929 (1999).
[12] J. Z. H Zhang and W. H. Miller, J. Chem. Phys. **91**, 1528 (1991).
[13] M. Zhao, D. G. Truhlar, D. W. Schwenke, and D. J. Kouri, J. Phys. Chem. **94**, 7074 (1990);
[14] M. J. D'Mello, D. E. Manolopoulos, and R. E. Wyatt, J. Chem. Phys. **94**, 5985 (1991).
[15] R. T Pack and G. A. Parker, J. Chem. Phys. **87**, 3888 (1987).
[16] D. Skouteris, J. F. Castillo, and D. E. Manolopolous, Comput. Phys. Commun. **113**, 128 (2000).
[17] Y.-S. M. Wu, A. Kuppermann, and B. Lepetit, Chem. Phys. Lett. **186**, 319 (1991).
[18] S. Hochman-Kowal and A. Persky, Chem. Phys. **222**, 29 (1997).
[19] A. J. C. Varandas and H. G. Yu, J. Mol. Struct.: THEOCHEM **81**, 4933 (1999).
[20] D. C. Chatfield, S. L. Mielke, T. C. Allison, and D. G. Truhlar, J. Chem. Phys. **112**, 8387 (2000); in *Dynamics of Molecules and Chemical Reactions*, edited by R. E. Wyatt and J. Z. H. Zhang (Dekker, New York, 1996), p. 323.
[21] S. D. Chao, S. A. Harich, D. X. Dai, C. C. Wang, X. Yang, and R. T. Skodje (unpublished).
[22] C. A. Mead and D. G. Truhlar, J. Chem. Phys. **70**, 2284 (1979).
[23] Y. S. M. Wu and A. Kuppermann, Chem. Phys. Lett. **235**, 105 (1995); **201**, 178 (1993); A. Kuppermann, in *Dynamics of Molecules and Chemical Reactions*, edited by R. E. Wyatt and J. Z. H. Zhang (Dekker, New York, 1996), p. 411.
[24] D. A. V. Kliner, D. E. Adelman, and R. N. Zare, J. Chem. Phys. **95**, 1648 (1991).
[25] A. Kuppermann and Y.-S. M. Wu, Chem. Phys. Lett. **205**, 577 (1993); **213**, 636(E) (1993).
[26] B. K. Kendrick, J. Chem. Phys. **112**, 5679 (2000); **114**, 4335(E) (2001).
[27] A. Kuppermann and Y.-S. M. Wu, Chem. Phys. Lett. **349**, 537 (2001).
[28] F. Fernandez-Alonso and R. N. Zare, Annu. Rev. Phys. Chem. **53**, 67 (2002).
[29] G. C. Schatz, Science **288**, 1599 (2000).
[30] D. G. Truhlar and A. Kuppermann, J. Chem. Phys. **56**, 2232 (1972).
[31] R. D. Levine and S.-F. Wu, Chem. Phys. Lett. **11**, 557 (1971).
[32] D. M. Neumark, A. M. Wodke, G. N. Robinson, C. C. Hayden, R. Shobatake, R. K. Sparks, T. P. Schafer, and Y. T. Lee, J. Chem. Phys. **82**, 3045 (1985).
[33] R. T. Skodje, D. Skouteris, D. E. Manolopoulos, S.-H. Lee, F. Dong, and K. Liu, J. Chem. Phys. **112**, 4536 (2000).
[34] R. T. Skodje, D. Skouteris, D. E. Manolopoulos, S.-H. Lee, F. Dong, and K. Liu, Phys. Rev. Lett. **85**, 1206 (2000).
[35] S. A. Cuccaro, P. G. Hipes, and A. Kuppermann, Chem. Phys. Lett. **157**, 440 (1989).
[36] M. S. Zhao, M. Mladenovic, D. G. Truhlar, D. W. Schwenke, O. Sharafeddin, Y. Yan, and D. J. Kouri, J. Chem. Phys. **91**, 5302 (1989).
[37] R. T. Skodje, R. Sadeghi, H. Koppel, and J. L. Krause, J. Chem. Phys. **101**, 1725 (1994).
[38] A. Kuppermann and Y.-S. M. Wu, Chem. Phys. Lett. **241**, 229 (1995); **243**, 586(E) (1995).
[39] W. H. Miller and J. Z. H. Zhang, J. Phys. Chem. **95**, 12 (1991).
[40] F. J. Aoiz, V. J. Herrero, and V. S. Rabanos, J. Chem. Phys. **97**, 7423 (1994).
[41] B. K. Kendrick, L. Jayasinghe, S. Moser, M. Auzinsh, and N. Shafer-Ray, Phys. Rev. Lett. **84**, 4325 (2000); **86**, 2482(E) (2001).
[42] S. D. Chao and R. T. Skodje, Chem. Phys. Lett. **336**, 364 (2001).
[43] F. J. Aoiz, L. Banares, and J. F. Castillo, J. Chem. Phys. **114**, 8237 (2001).
[44] B. K. Kendrick, J. Chem. Phys. **114**, 8796 (2001).
[45] F. Fernandez-Alonso, B. D. Bean, J. D. Ayers, A. E. Pomerantz, R. N. Zare, L. Banares, and F. J. Aoiz, Angew. Chem. Int. Ed. Engl. **39**, 2748 (2000).
[46] T. C. Allison, R. S. Friedman, D. J. Kaufman, and D. G. Truhlar, Chem. Phys. Lett. **327**, 439 (2000).
[47] S. A. Harich, D. Dai, X. Yang, S. D. Chao, and R. T. Skodje, J. Chem. Phys. **116**, 4769 (2002).
[48] S. A. Harich, D. Dai, C. C. Wang, X. Yang, S. D. Chao, and R. T. Skodje, Nature **419**, 281 (2002).
[49] K. D. Rinnen, D. A. V. Kliner, M. A. Buntine, and R. N. Zare, Chem. Phys. Lett. **169**, 365 (1990).
[50] L. Schnieder, W. Meier, E. Wrede, K. H. Welge, M. N. R. Ashfold, and C. M. Western, J. Chem. Phys. **92**, 7027 (1990).
[51] X. Liu, J. J. Lin, S. A. Harich, G. C. Schatz, and X. Yang, Science **289**, 1536 (2000).
[52] X. Liu, J. J. Lin, S. A. Harich, and X. Yang, Phys. Rev. Lett. **86**, 408 (2001).
[53] J. P. Marangos, N. Shen, H. Ma, M. H. R. Hutchinson, and J. P. Connerade, J. Opt. Soc. Am. B **7**, 1254 (1990).
[54] J. F. Castillo, D. E. Manolopoulos, K. Stark, and H.-J. Werner, J. Chem. Phys. **104**, 6531 (1996).
[55] G. C. Schatz, Chem. Phys. Lett. **150**, 92 (1988).
[56] G. A. Parker and R. T Pack, J. Chem. Phys. **98**, 6883 (1993).
[57] D. E. Manolopoulos, J. Chem. Phys. **85**, 6425 (1986).
[58] J. Z. H. Zhang, J. Chem. Phys. **94**, 6047 (1991).
[59] A. Kuppermann, G. C. Schatz, and M. Baer, J. Chem. Phys. **65**, 4622 (1976).
[60] W. H. Miller, N. C. Handy, and J. E. Adams, J. Chem. Phys. **72**, 99 (1980).
[61] A. D. Isaacson and D. G. Truhlar, J. Chem. Phys. **76**, 1380 (1982).
[62] D. G. Truhlar, B. C. Garrett, and J. S. Klippenstein, J. Phys. Chem. **100**, 12771 (1996).
[63] S. K. Kim, E. R. Lovejoy, and C. B. Moore, J. Chem. Phys. **102**, 3202 (1995).
[64] S. Sukiasyan and H.-D. Meyer, J. Phys. Chem. A **105**, 2604 (2001).
[65] R. D. Levine, J. Phys. Chem. **94**, 8872 (1990).
[66] R. Sadeghi and R. T. Skodje, J. Chem. Phys. **102**, 193 (1995); **99**, 5126 (1993); Phys. Rev. A **52**, 1996 (1995).
[67] R. S. Friedman and D. G. Truhlar, Chem. Phys. Lett. **183**, 539 (1991).

Downloaded 12 Jul 2006 to 203.250.225.116. Redistribution subject to AIP license or copyright, see http://jcp.aip.org/jcp/copyright.jsp